Inorganic Chemistry

Article

pubs.acs.org/IC

Proton-Induced Reversible Modulation of the Luminescent Output of Rhenium(I), Iridium(III), and Ruthenium(II) Tetrazolate Complexes

Melissa V. Werrett,[†] Sara Muzzioli,[‡] Phillip J. Wright,[†] Antonio Palazzi,[‡] Paolo Raiteri,[†] Stefano Zacchini,[‡] Massimiliano Massi,*[,†] and Stefano Stagni*[,‡]

[†]Department of Chemistry, Curtin University, GPO Box U 1987, Perth, Australia, 6845

[‡]Department of Industrial Chemistry "Toso Montanari", University of Bologna, Viale Risorgimento 4, I-40136 Bologna, Italy

Supporting Information

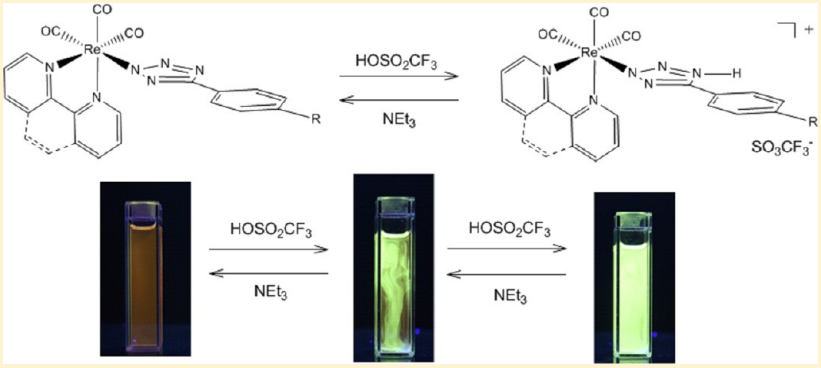

ABSTRACT: One of the distinct features of metal−tetrazolate complexes is the possibility of performing electrophilic additions onto the imine-type nitrogens of the coordinated five-membered ring. These reactions, in particular, provide a useful tool for varying the main structural and electronic properties of the starting tetrazolate complexes. In this paper, we demonstrate how the use of a simple protonation−deprotonation protocol enables us to reversibly change, to a significant extent, the light-emission output and performance of a series of Re(I)-tetrazolate-based phosphors of the general formulation *fac*-[Re(N^N)(CO)$_3$L], where N^N denotes diimine-type ligands such as 2,2′-bipyridine (bpy) or 1,10-phenanthroline (phen) and L represents a series of different 5-aryl tetrazolates. Indeed, upon addition of triflic acid to these neutral Re(I) complexes, a consistent blue shift ($\Delta\lambda_{max}$ ca. 50 nm) of the emission maximum is observed and the protonated species also display increased quantum yield values (4−13 times greater than the starting compounds) and longer decay lifetimes. This alteration can be reversed to the initial condition by further treating the protonated Re(I) complex with a base such as triethylamine. Interestingly, the reversible modulation of luminescent features by the same protonation−deprotonation mechanism appears as a quite general characteristic of photoactive metal tetrazolate complexes, even for compounds in which the 2-pyridyl tetrazolate ligands coordinate the metal center with a bidentate mode, such as the corresponding Ir(III) cyclometalates [Ir(C^N)$_2$L] and the Ru(II) polypyridyl derivatives [Ru(bpy)$_2$L]$^+$. In these cases, the protonation of the starting materials leads to red-shifted and more intense emissions for the Ir(III) complexes, while almost complete quenching is observed in the case of the Ru(II) analogues.

INTRODUCTION

Among the reasons that might explain the tremendous scientific developments in the chemistry of some specific classes of octahedral d^6 metal complexes, namely, Ru(II) polypyridyls, cyclometalated Ir(III) derivatives, and tricarbonyl Re(I) diimines, the modulation of their photophysical properties by variation of the set of the coordinated ligands is of crucial importance. In particular, the relevance of the role played by the coordinated ligands is evident when considering that the photophysical behavior of Ru(II) polypyridyls, which represent the paradigm of luminescent metal complexes, is governed by metal-to-ligand charge transfer (MLCT) excited states.[1] The contribution of the ligands in determining the nature of the excited states becomes even more appreciable on passing to isoelectronic complexes containing third-row transition metal ions such as tricarbonyl Re(I) diimines[2] and, to a greater extent, cyclometalated Ir(III) derivatives.[3] Overall, the synergistic effect that arises from the combination of the "right" metal with the appropriately modified set of ligands has driven the application of these classes of photoactive d^6 metal complexes in some of the most challenging research fields: these include the conversion of solar energy,[4] the design of emitting molecules for lighting devices and displays,[5] the development of new luminescent markers and probes for biological imaging,[6] and, to a more general meaning, the proposition of new families of luminescent sensors.[7] In the latter context, the sensing ability of metal complexes—which is meant herein as the variation of

Received: August 27, 2013
Published: December 20, 2013

the luminescence output induced by external stimuli—can be achieved by different mechanisms that might involve the occurrence of proton-coupled electron transfer (PCET)[8] or the quenching of the emission originating from triplet excited states (e.g., O_2 sensors)[9] or from the analyte-induced perturbation of the "actor" ligand influencing the emissive excited state.[10] In particular, following our work centered on the study of the coordination chemistry of tetrazolate ligands in Ru(II) polypyridyls,[11] Ir(III)cyclometalates,[12] Re(I)-diimine,[13] and Pt(II)-cyclophane compounds,[14] we could observe how, in all cases, the tetrazolate ligands actually behaved as "actor" ligands, since their role in determining electronic properties and, in particular, the luminescent performances of the corresponding complexes was of relevant importance. From this point of view, an emblematic example is represented by the series of tetrazolate-based Ir(III) cyclometalates.[12] In those cases, the tuning of the emitted color spans over a 100 nm range and could be induced by introducing different substituted tetrazolates in the structure of the corresponding Ir(III) cyclometalated fragments. The color variation efficiently demonstrates the participation of the tetrazolate ligand in the composition of the emitting MLCT states. As a consequence, any reversible or irreversible modification occurring to the coordinated tetrazolate moieties might lead to the further modulation of the luminescent properties of the corresponding complexes. This behavior was observed in our investigation both for the Ru(II) and, particularly, for the Ir(III) tetrazolate complexes we have reported so far,[11,12] in which the regioselective addition of a methyl group to the coordinated tetrazolate ring resulted in the enhancement of emission intensity and shift of the emission maxima. Similarly, we described how methylation influences the quantum yield of square-planar Pt(II) tetrazolate complexes.[14] It has to be pointed out that all these modifications displayed an irreversible character. The opportunity to extend similar effects in a reversible manner prompted us to perform protonation and deprotonation reactions onto tricarbonyl Re(I) diimine tetrazolate derivatives of the general formula *fac*-[Re(N^N)$(CO)_3$L] (see Scheme 1), for which no studies dealing with their reactivity toward electrophilic agents has been reported yet. In order to determine whether the reversible switching of the luminescence output that was displayed by Re(I) tetrazolate complexes might represent a general and peculiar feature of luminescent metal tetrazolate species, we have also extended this study to the cases of the isoelectronic Ir(III) cyclometalated and Ru(II) polypyridyl tetrazolate complexes.

Scheme 1. Complexes and Their Acronyms

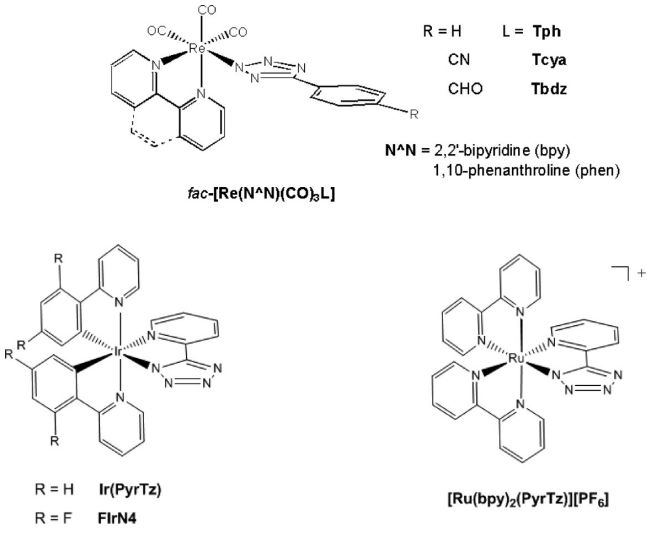

RESULTS AND DISCUSSION

Spectroscopic Characterization. All of the starting neutral Re(I) complexes were synthesized using a method differing from the ones previously reported.[13a,c] The method does not involve the use of a silver salt for halogen abstraction, rather just a solvent mixture of ethanol/water (75:25 v/v) in the presence of triethylamine. In most cases the complexes were simply filtered off after 24 h at reflux and did not require further purification; if purification was required, it was accomplished with the use of flash chromatography. By following this procedure, the new *fac*-[Re(bpy)$(CO)_3$Tcya] complex was prepared and characterized spectroscopically. Moreover, its structure has been confirmed via X-ray crystallography (Figure S1 and Table S1, Supporting Information). The geometry and bonding parameters of *fac*-[Re(bpy)$(CO)_3$Tcya] are in agreement with those previously reported for analogous neutral complexes.[13a]

The protonation reactions (Scheme 2) have been performed by adding a slight excess (ca. 1.5 equiv) of triflic acid to dichloromethane solutions of the starting neutral Re(I) tetrazolate complexes maintained at −50 °C.

In contrast with that reported by Szczepura and co-workers in the case of the addition of HBF_4 to hexanuclear Re(III) clusters containing 5-aryl tetrazolate moieties,[15] the protonation of the tricarbonyl Re(I) diimine tetrazolate complexes described herein occurred even at low temperature. In particular, all the protonation procedures could be monitored by solution-state IR spectroscopy. Indeed, the formation of the targeted protonated species was witnessed by the shift toward higher wavenumbers of the CO stretchings on passing from the neutral to the cationic complexes. In all cases, the *facial* configuration of the CO ligands was retained. This appeared evident by considering that, apart from the expected shift of the CO bands, the profile of each IR spectrum—that always consisted of one sharp band centered at ca. 2040 cm^{-1}, assigned to the totally symmetric in-phase stretching A′(1), and a broader one at ca. 1937 cm^{-1} that is the result of the superimposition of the totally symmetric out-of-phase stretching A′(2) and the asymmetric stretching A″ (Figure 1 and Table 1)—did not change upon protonation.

The protonated Re(I) complexes were then characterized by ^1H and ^{13}C NMR spectroscopy, and the comparative analysis of the obtained spectra with those of each starting complex indicated that, as expected, the addition of H^+ is directed to the coordinated tetrazolate, which behaves as a Brønsted-type base. On comparing the corresponding starting and protonated Re(I) complexes (see Supporting Information, Figures S2−S7), it is possible to observe that the most evident variations occurring upon protonation are localized on the phenyl ring conjugated with the tetrazole group. Taken together, these spectroscopic features suggest that the protonation reaction occurs chemoselectively to the tetrazolate ligand. Also, on the basis of our previous studies dealing with the protonation of a series of $[Ru(tpy)(bpy)L]^+$ complexes, in which the tetrazolate ligands adopt the same monocoordinate binding mode, we assume that the N(4) atom of the coordinated tetrazolate ring likely represents the privileged site where the electrophilic attack occurs. Reliable evidence for such regioselective

dx.doi.org/10.1021/ic402187e | Inorg. Chem. 2014, 53, 229−243

Scheme 2. Protonation Reaction of the Re(I)-Tetrazolate Complexes and Atom Labeling

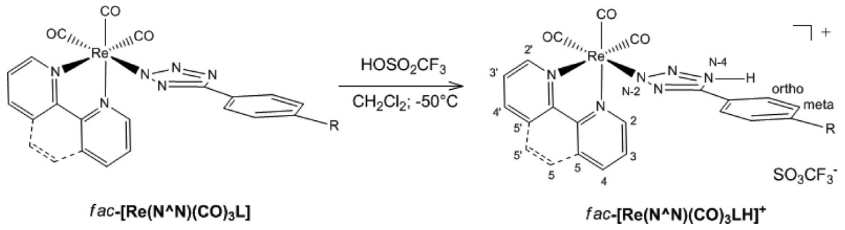

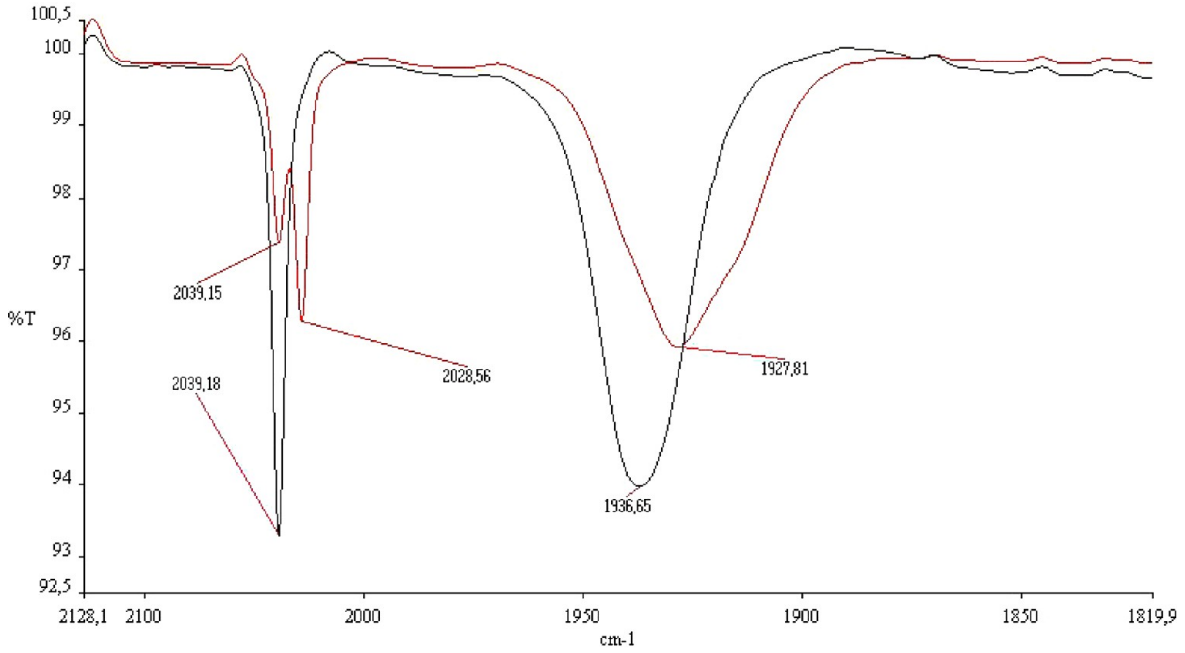

Figure 1. Monitoring the protonation of *fac*-[Re(bpy)(CO)$_3$Tph]: solution IR spectra showing the CO stretchings pattern of the protonated compound *fac*-[Re(bpy)(CO)$_3$TphH]$^+$ (black trace) compared to those of the mixture containing both the protonated species and the neutral starting complex *fac*-[Re(bpy)(CO)$_3$Tph] (red trace).

Table 1. Stretching Frequencies (cm^{-1}) of the CO Bands of All the Re(I) Complexes Reported in This Work[a]

	CO A′(1)	CO A′(2)/A″
fac-[Re(phen)(CO)$_3$Tph]	2029	1922
fac-[Re(phen)(CO)$_3$TphH]$^+$	2039	1936
fac-[Re(bpy)(CO)$_3$Tph]	2029	1924
fac-[Re(bpy)(CO)$_3$TphH]$^+$	2039	1936
fac-[Re(phen)(CO)$_3$Tbdz]	2029	1923
fac-[Re(phen)(CO)$_3$TbdzH]$^+$	2040	1938
fac-[Re(bpy)(CO)$_3$Tbdz]	2029	1922
fac-[Re(bpy)(CO)$_3$TbdzH]$^+$	2040	1937
fac-[Re(phen)(CO)$_3$Tcya]	2030	1923
fac-[Re(phen)(CO)$_3$TcyaH]$^+$	2040	1937
fac-[Re(bpy)(CO)$_3$Tcya]	2029	1923
fac-[Re(bpy)(CO)$_3$TcyaH]$^+$	2040	1938

[a]Values are relative to solution-state (dichloromethane as the solvent) IR spectra recorded at room temperature.

protonation might be obtained from the analysis of the ^{13}C NMR spectra, in which the tetrazole carbon (Ct) resonance should be found in the 154−158 ppm[16,11d,f] chemical shift range, which is diagnostic for the presence of a substituent at the N(4) atom. Unfortunately, for the majority of the protonated species the Ct resonance could not be detected in the ^{13}C NMR spectra, neither in the expected chemical shift range nor in the one typical of the starting compounds (δCt = 161−165 ppm). However, quite decisive support of our hypothesis came from the analysis of the structures of the Re(I) protonated complexes obtained by X-ray diffraction, whose detailed descriptions are given in the following section.

Crystal Structures. The molecular structures of the *fac*-[Re(phen)(CO)$_3$TphH]$^+$, *fac*-[Re(phen)(CO)$_3$TcyaH]$^+$, *fac*-[Re(phen)(CO)$_3$TbdzH]$^+$, *fac*-[Re(bpy)(CO)$_3$TcyaH]$^+$, and *fac*-[Re(bpy)(CO)$_3$TbdzH]$^+$ cationic complexes have been determined by single-crystal X-ray diffractometry on their *fac*-[Re(phen)(CO)$_3$TphH][CF$_3$SO$_3$] (Figure 2), *fac*-[Re(phen)(CO)$_3$TphH][CF$_3$SO$_3$]·0.25Et$_2$O (Figure 3), *fac*-[Re(phen)(CO)$_3$TcyaH][CF$_3$SO$_3$] and *fac*-[Re(phen)(CO)$_3$TbdzH][CF$_3$SO$_3$] (Supporting Information, Figures S8 and S9, respectively), *fac*-[Re(bpy)(CO)$_3$TcyaH][CF$_3$SO$_3$] (Figure 4), and *fac*-[Re(bpy)(CO)$_3$TbdzH][CF$_3$SO$_3$] (Figure 5) salts. A selection of the most relevant bonding and angle parameters is reported in Table 2. The structure of *fac*-[Re(phen)(CO)$_3$TphH]$^+$ has been determined both in *fac*-[Re(phen)(CO)$_3$TphH][CF$_3$SO$_3$] (Figure 2) and in the solvate *fac*-[Re(phen)(CO)$_3$TphH][CF$_3$SO$_3$]·0.25Et$_2$O (Figure 3). The Re centers in all the complexes display an octahedral geometry, being coordinated to three CO ligands (in a relative *fac* arrangement), a *cis*-chelating dinitrogen ligand, and an aryl-substituted protonated tetrazolate ring. The tetrazolate ligand is bound to the Re center through N(2), and protonation occurs

dx.doi.org/10.1021/ic402187e | *Inorg. Chem.* 2014, 53, 229−243

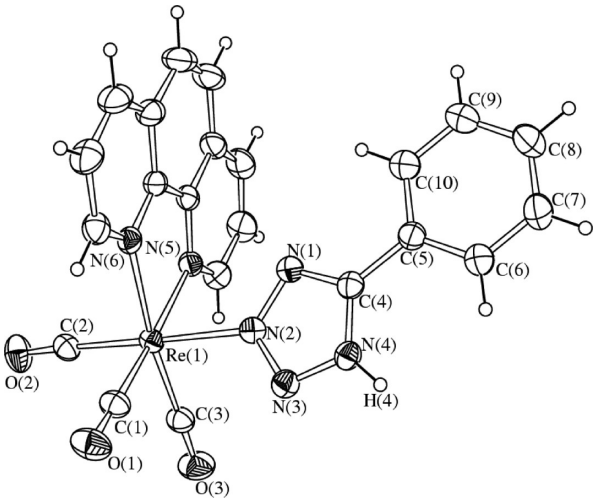

Figure 2. Molecular structure of *fac*-[Re(phen)$(CO)_3$TphH]-[CF_3SO_3] with key atoms labeled. Displacement ellipsoids are at the 30% probability level. The $[CF_3SO_3]^-$ anion is omitted for clarity.

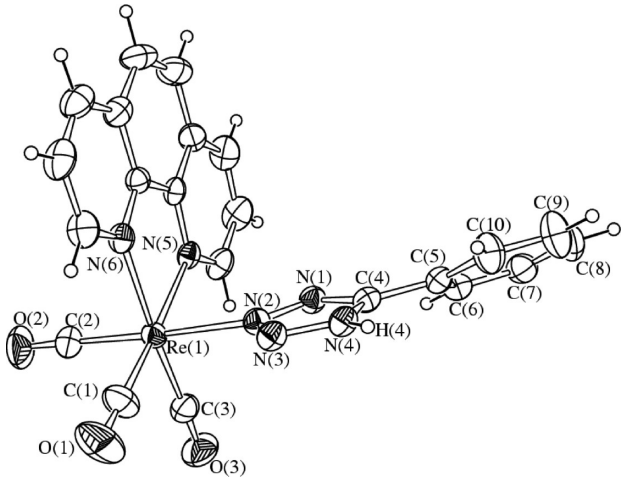

Figure 3. Molecular structure of *fac*-[Re(phen)$(CO)_3$TphH]-[CF_3SO_3]·0.25Et_2O with key atoms labeled. Displacement ellipsoids are at the 30% probability level. The $[CF_3SO_3]^-$ anion and the Et_2O molecule are omitted for clarity.

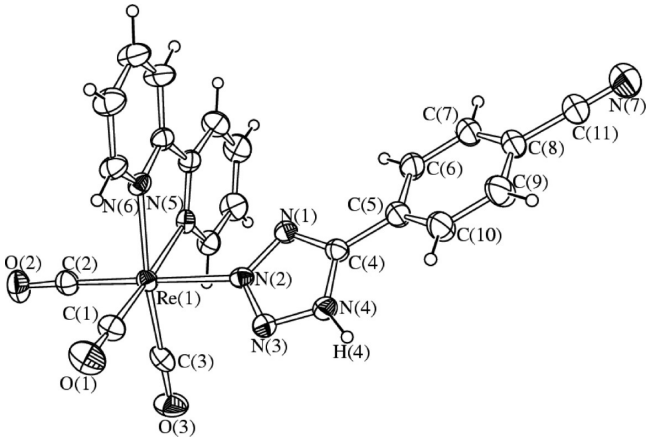

Figure 4. Molecular structure of *fac*-[Re(bpy)$(CO)_3$TcyaH][CF_3SO_3] with key atoms labeled. Displacement ellipsoids are at the 30% probability level. The $[CF_3SO_3]^-$ anion is omitted for clarity.

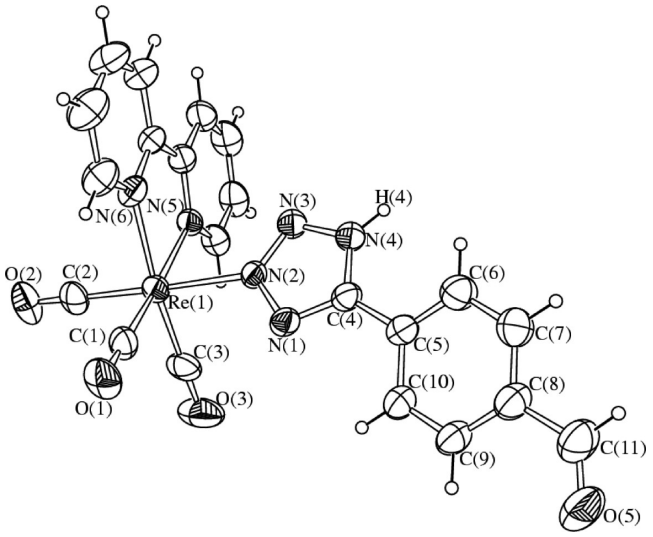

Figure 5. Molecular structure of *fac*-[Re(bpy)$(CO)_3$TbdzH][CF_3SO_3] with key atoms labeled. Displacement ellipsoids are at the 30% probability level. The $[CF_3SO_3]^-$ anion is omitted for clarity.

always at N(4) as previously found in analogous Ru(II) complexes.[11a,c] Also the bonding parameters determined for the aryl-substituted protonated tetrazolate rings compare very well to those previously found in the protonated Ru(II) complexes. The five-membered tetrazole rings are perfectly planar [mean deviations from the N(1) N(2) N(3) N(4) C(4) least-squares planes in the range 0.0016−0.0071 Å].

Conversely, the N(1)−C(4)−C(5)−C(6) torsion angles are very different in the six crystal structures, i.e., −172.4(3)° in *fac*-[Re(phen)$(CO)_3$TphH][CF_3SO_3], −25.2(6)° in *fac*-[Re(phen)$(CO)_3$TphH][CF_3SO_3]·0.25Et_2O, −1.9(6)° in *fac*-[Re(phen)$(CO)_3$TcyaH][CF_3SO_3], 2.4(10)° in *fac*-[Re(phen)$(CO)_3$TbdzH][CF_3SO_3], −21.0(10)° in *fac*-[Re(bpy)$(CO)_3$TcyaH][CF_3SO_3], and −160.4(7)° in *fac*-[Re(bpy)$(CO)_3$TbdzH][CF_3SO_3]. An absolute value of this torsion angle close to 0° or 180° indicates coplanarity between the protonated tetrazolate and aryl ring, whereas significant deviations from these values are indicative of loss of coplanarity. The fact that the experimental values are rather spread and, in particular, the fact that for the same *fac*-[Re(phen)$(CO)_3$TphH]$^+$ cation two very different torsion angles have been found in the *fac*-[Re(phen)$(CO)_3$TphH][CF_3SO_3] (−172.4(3)°) and *fac*-[Re(phen)$(CO)_3$TphH][CF_3SO_3]·0.25Et_2O (−25.2(6)°) salts suggest that the relative orientations of the protonated tetrazolate and aryl rings in the solid state are mainly determined by packing effects rather than by electronic conjugation. In particular, in all six crystal structures H-bonds are present involving the N(4)−H(4) group as a donor and the O atoms of the $[CF_3SO_3]^-$ anions as acceptors (Table 3). Similarly, the orientation of the aryl-substituted protonated tetrazolate ligand with respect to the Re(phen)$(CO)_3$ framework is very different in the six crystal structures (see C(2)−Re(1)−N(2)−N(1) torsion angle in Table 2), suggesting free rotation around the Re(1)−N(2) bond in solution, whereas the geometry found in the solid state is determined by H-bonds and other crystal-packing effects.

Photophysical Properties. The relevant absorption and emission data of all the complexes are listed in Tables 4 and 5.

The UV−vis absorption profiles of the Re(I) compounds reported herein are quite similar for all the complexes, with

dx.doi.org/10.1021/ic402187e | *Inorg. Chem.* 2014, 53, 229−243

Table 2. Selected Bond Lengths (Å) and Angles (deg) for *fac*-[Re(phen)(CO)$_3$TphH][CF$_3$SO$_3$] (1), *fac*-[Re(phen)(CO)$_3$TphH][CF$_3$SO$_3$]·0.25Et$_2$O (2), *fac*-[Re(phen)(CO)$_3$TcyaH][CF$_3$SO$_3$] (3), *fac*-[Re(phen)(CO)$_3$TbdzH][CF$_3$SO$_3$] (4), *fac*-[Re(bpy)(CO)$_3$TcyaH][CF$_3$SO$_3$] (5), and *fac*-[Re(bpy)(CO)$_3$TbdzH][CF$_3$SO$_3$] (6)

	1	2	3	4	5	6
Re(1)−C(1)	1.914(3)	1.911(5)	1.931(5)	1.920(8)	1.913(7)	1.912(8)
Re(1)−C(2)	1.922(3)	1.915(5)	1.907(4)	1.903(7)	1.890(8)	1.914(8)
Re(1)−C(3)	1.917(3)	1.910(5)	1.921(4)	1.924(10)	1.919(7)	1.910(9)
Re(1)−N(2)	2.182(2)	2.188(3)	2.193(3)	2.191(5)	2.168(5)	2.190(5)
Re(1)−N(5)	2.172(2)	2.168(3)	2.183(3)	2.187(5)	2.174(5)	2.161(5)
Re(1)−N(6)	2.169(2)	2.182(3)	2.183(3)	2.195(6)	2.181(5)	2.160(6)
C(1)−O(1)	1.150(4)	1.149(6)	1.146(6)	1.139(8)	1.151(7)	1.160(9)
C(2)−O(2)	1.140(4)	1.141(6)	1.142(5)	1.151(7)	1.170(8)	1.154(9)
C(3)−O(3)	1.142(4)	1.149(6)	1.146(5)	1.141(10)	1.150(8)	1.156(9)
N(1)−N(2)	1.345(3)	1.349(5)	1.358(4)	1.359(7)	1.347(7)	1.349(7)
N(2)−N(3)	1.300(3)	1.298(4)	1.294(4)	1.286(7)	1.317(7)	1.296(7)
N(3)−N(4)	1.330(3)	1.333(5)	1.335(4)	1.336(7)	1.324(7)	1.341(7)
N(1)−C(4)	1.322(4)	1.328(5)	1.324(5)	1.322(7)	1.315(8)	1.324(8)
C(4)−N(4)	1.336(4)	1.335(5)	1.334(5)	1.312(8)	1.333(7)	1.348(8)
C(4)−C(5)	1.464(4)	1.462(6)	1.461(5)	1.478(8)	1.466(9)	1.452(9)
Re(1)−C(1)−O(1)	179.3(3)	178.6(5)	179.4(5)	178.2(7)	177.8(7)	179.1(7)
Re(1)−C(2)−O(2)	177.6(3)	178.4(5)	176.6(4)	177.5(7)	179.2(6)	179.1(6)
Re(1)−C(3)−O(3)	179.3(3)	176.7(5)	178.2(4)	178.6(9)	177.4(6)	178.6(9)
C(1)−Re(1)−N(5)	172.45(11)	172.57(19)	171.81(16)	171.9(3)	173.2(2)	173.2(3)
C(2)−Re(1)−N(2)	178.71(11)	177.13(17)	175.60(15)	175.8(2)	179.7(2)	177.4(2)
C(3)−Re(1)−N(6)	172.58(11)	172.55(18)	172.86(15)	173.7(3)	172.7(2)	172.7(3)
N(5)−Re(1)−N(6)	75.83(9)	75.77(12)	75.34(11)	75.29(19)	74.30(18)	75.0(2)
sum of angles at N$_4$C	540.0(5)	540.0(7)	540.0(7)	540.0(11)	540.0(11)	539.9(11)
sum of angles at C(4)	359.9(5)	360.0(7)	359.9(5)	359.9(10)	359.9(10)	360.0(10)
N(1)−C(4)−C(5)−C(6)	−172.4(3)	−25.2(6)	−1.9(6)	2.4(10)	−21.0(10)	−160.4(7)
C(2)−Re(1)−N(2)−N(1)	−1(5)	157.0(3)	24.2(3)	66.4(5)	−147.7(5)	32.0(5)

Table 3. Hydrogen Bonds for *fac*-[Re(phen)(CO)$_3$TphH][CF$_3$SO$_3$], *fac*-Re(phen)(CO)$_3$TphH][CF$_3$SO$_3$]·0.25Et$_2$O, *fac*-[Re(phen)(CO)$_3$TcyaH][CF$_3$SO$_3$], *fac*-[Re(phen)(CO)$_3$TbdzH][CF$_3$SO$_3$], *fac*-[Re(bpy)(CO)$_3$TcyaH][CF$_3$SO$_3$], and *fac*-[Re(bpy)(CO)$_3$TbdzH][CF$_3$SO$_3$]

	d(N−H)	*d*(H···O)	*d*(N···O)	∠(NHO)
fac-[Re(phen)(CO)$_3$TphH][CF$_3$SO$_3$]	0.863(18)	1.818(19)	2.681(3)	179(3)
fac-[Re(phen)(CO)$_3$TphH][CF$_3$SO$_3$]·0.25Et$_2$O	0.873(19)	1.88(2)	2.752(4)	175(4)
fac-[Re(phen)(CO)$_3$TcyaH][CF$_3$SO$_3$]	0.85(2)	1.87(2)	2.720(4)	175(4)
fac-[Re(phen)(CO)$_3$TbdzH][CF$_3$SO$_3$]	0.86	1.89	2.729(7)	164(4)
fac-[Re(bpy)(CO)$_3$TcyaH][CF$_3$SO$_3$]	0.87(2)	1.88(3)	2.732(7)	168(6)
fac-[Re(bpy)(CO)$_3$TbdzH][CF$_3$SO$_3$]	0.87(2)	1.80(2)	2.673(8)	176(7)

intense ligand-centered (LC) $\pi-\pi^*$ transitions occurring in the high-energy UV region and weaker charge transfer (CT) bands tailing in the visible part of the spectrum. When compared to the initial neutral complexes, the UV−vis absorption spectra of the protonated cationic compounds display the expected hypsochromic shift of the MLCT transition, which is accompanied by an analogous variation of the LC-based absorption bands (see Figure 6 and Figures S10−S13, Supporting Information). This behavior can be rationalized by considering that the protonation of the tetrazolate ring reduces the overall electron density on the rhenium center. The reduction is likely to be caused by the decreased σ donation and/or increased π acceptance of the protonated tetrazolate. The overall effect is hence a stabilization of the 5d orbitals on the metal with consequent widening of the HOMO−LUMO gap.

If the changes of the absorption features occurring upon protonation were somewhat expected, the extent of the modifications of the luminescence properties was actually surprising. Upon excitation of the ^{1}MLCT band at ca. 370 nm, each of the starting neutral Re(I) complexes display a single broad and featureless orange-red emission centered between 584 nm (as for complexes *fac*-[Re(phen)(CO)$_3$Tbdz] and *fac*-[Re(phen)(CO)$_3$Tcya]) and 606 nm (*fac*-[Re(bpy)-(CO)$_3$Tph]). According to our previous studies,[13] the phosphorescent emission originates from excited states of triplet metal−ligand-to-ligand charge transfer (^{3}MLLCT) nature, where the main contributors to the HOMO-type orbitals involved in the lowest energy transitions are the metal 5d and the tetrazolate π system and the main contributor for the LUMO-type orbitals is the π^* system of the diimine ligand. The conversion of the neutral Re(I) tetrazolate complexes into their conjugated acids dramatically changes the luminescence properties, in a similar manner for both the bpy and phen complexes. Indeed, the moderately intense orange-red emission of the neutral compounds shifts to a bright green color, with emission maxima blue-shifted of ca. 50 nm (Table 4 and Figures 7 and 8).

This behavior might be explained as a protonation-mediated reduction, or complete removal, of the contribution of the tetrazolate ligand in the composition of the emitting excited states. Indeed, we have previously observed[13a] the same blue-

dx.doi.org/10.1021/ic402187e | *Inorg. Chem.* 2014, 53, 229−243

Table 4. Absorption and Emission Spectral Data of All the Re(I) Complexes[a]

	absorption	emission 298 K[b,c]				emission 77 K[c,d]	
complex	λ_{max} (nm); $10^{-4}\varepsilon$ (M^{-1} cm^{-1})	λ (nm)	τ (μs) dear	τ (μs) air	Φ dear	Φ air	λ (nm)	τ (μs)
[Re(phen)$(CO)_3$Tph]	259 (1.560) 363 (0.196)	592	0.517	0.268	0.072	0.045	534	6.75
[Re(phen)$(CO)_3$TphH]$^+$	254 (1.325) 335 (0.240)	538	2.505	1.293	0.470	0.328	500	5.25
[Re(bpy)$(CO)_3$Tph]	251 (1.570) 285 (0.895) 373 (0.166)	606	0.092	0.085	0.030	0.028	528	2.97
[Re(bpy)$(CO)_3$TphH]$^+$	245 (1.556) 319 (0.520) 352 (0.185)	548	0.660	0.596	0.135	0.120	502	3.54
[Re(phen)$(CO)_3$Tcya]	274 (1.115) 360 (0.114)	584	0.518	0.382	0.070	0.060	528	6.75
[Re(phen)$(CO)_3$TcyaH]$^+$	257 (1.650) 342 (0.180)	534	2.948	1.819	0.540	0.296	508	5.42
[Re(bpy)$(CO)_3$Tcya]	284 (0.890) 369 (0.090)	598	0.139	0.107	0.025	0.021	526	3.64
[Re(bpy)$(CO)_3$TcyaH]$^+$	254 (1.010) 319 (0.310) 350 (0.120)	546	0.874	0.655	0.204	0.103	534	2.32 (47) 4.74 (53)
[Re(phen)$(CO)_3$Tbdz]	272 (1.413) 366 (0.060)	584	0.775	0.343	0.053	0.043	516	8.00
[Re(phen)$(CO)_3$TbdzH]$^+$	272 (1.262) 351 (0.940)	534	2.186	1.333	0.206	0.105	496	9.57
[Re(bpy)$(CO)_3$Tbdz]	296 (1.020) 372 (0.120)	596	0.124	0.105	0.021	0.015	528	3.55
[Re(bpy)$(CO)_3$TbdzH]$^+$	266 (1.291) 319 (0.410)	546	0.825	0.612	0.276	0.145	502	3.38

[a]All data for complexes in 10^{-5} M CH_2Cl_2 solutions. [b]"Air" denotes air-equilibrated samples, "dear" means degassed (O_2-free) samples; quantum yields are measured versus rhodamine 101 in ethanol. [c]For the biexponential excited-state lifetimes (τ), the relative weights of the exponential curve are reported in parentheses. [d]In frozen CH_2Cl_2 matrixes.

Table 5. Absorption and Emission Spectral Data of All the Ir(III) and Ru(II) Complexes[a]

	absorption	emission 298 K[b,c]				emission 77 K[c,d]	
	λ_{max} (nm); $10^{-4}\varepsilon$ (M^{-1} cm^{-1})	λ (nm)	τ (μs) dear	τ (μs) air	Φ dear	Φ air	λ (nm)	τ (μs)
Ir(PyrTz)	258 (1.738) 391 (0.192)	484, 512	0.423	0.080	0.038	0.032	476, 510	3.58
[Ir(PyrTzH)]$^+$	253 (1.880) 385 (0.257)	594	0.158	0.100	0.102	0.057	477, 510	2.93
FIrN4	250 (1.520) 368 (0.200)	458, 488	0.161	0.105	0.056	0.034	450, 482	3.14 (26) 4.85 (74)
[FIrN4H]$^+$	239 (1.437) 303 (0.567)	536	0.351	0.226	0.182	0.138	448, 478	4.23
[Ru$(bpy)_2$(PyrTz)]$^+$	291 (1.701) 370 (0.272) 475 (0.311)	653[e]	0.220[e]	0.077[e]	n.d.[e]	0.004[e]	597[e]	5.23[e]
[Ru$(bpy)_2$(PyrTzH)]$^{2+}$	287 (1.515) 441 (0.346)	n.d.	n.d	n.d	n.d.	n.d.	n.d.	n.d.

[a]All data for complexes in 10^{-5} M CH_2Cl_2 solutions. [b]"Air" denotes air-equilibrated samples, "dear" means degassed (O_2 free) samples; quantum yields are measured versus quinine bisulfate in 1 N H_2SO_4. [c]For the biexponential excited-state lifetimes (τ), the relative weights of the exponential curve are reported in parentheses. [d]In frozen CH_2Cl_2 matrixes. [e]Data from ref 11e.

shift of the emission maxima by comparing the emission profiles of the neutral Re(I)-tetrazolate complexes of the type *fac*-[Re(bpy)$(CO)_3$L] with that of the corresponding solvate complex *fac*-[Re(bpy)$(CO)_3(CH_3CN)]^+$.[13a] This hypothesis is further corroborated by TD-DFT computational calculations (see next section).

In accordance with the energy gap law,[17] such a tremendously improved performance, the progress of which can be observed by partitioning the addition of triflic acid into several aliquots (Figure 8 and Figures S10–S13, Supporting Information), is at first evidenced by considering that the protonated compounds display quantum yield values (Φ) that are 4–13 times higher than those of the starting material. Also,

dx.doi.org/10.1021/ic402187e | Inorg. Chem. 2014, 53, 229–243

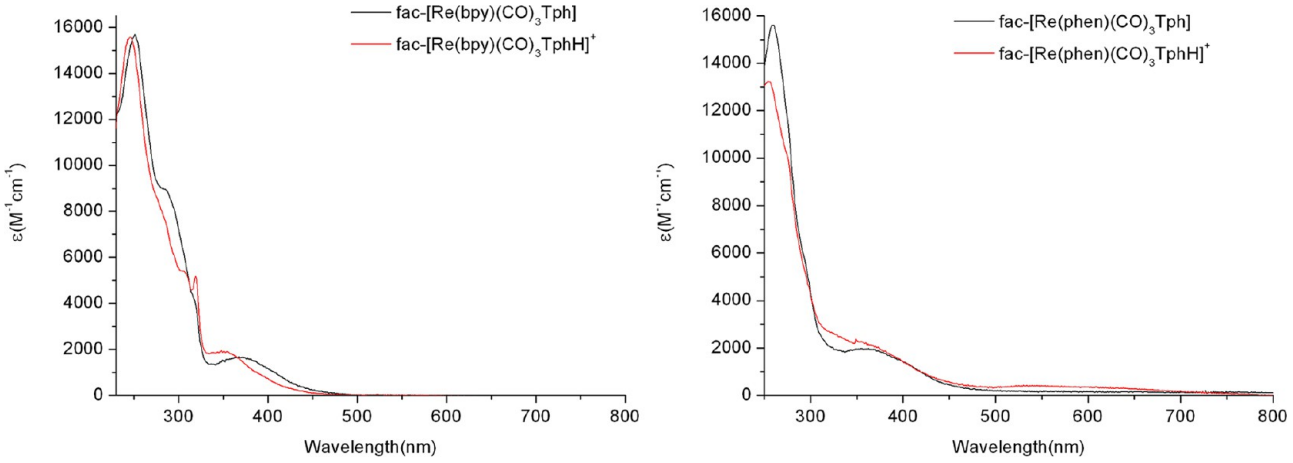

Figure 6. UV−vis absorption profiles of the protonated *fac*-[Re(N^N)$(CO)_3$TphH]$^+$ complexes—red traces; N^N = bpy (left), N^N = phen (right)—compared to those of the corresponding neutral precursors (black traces).

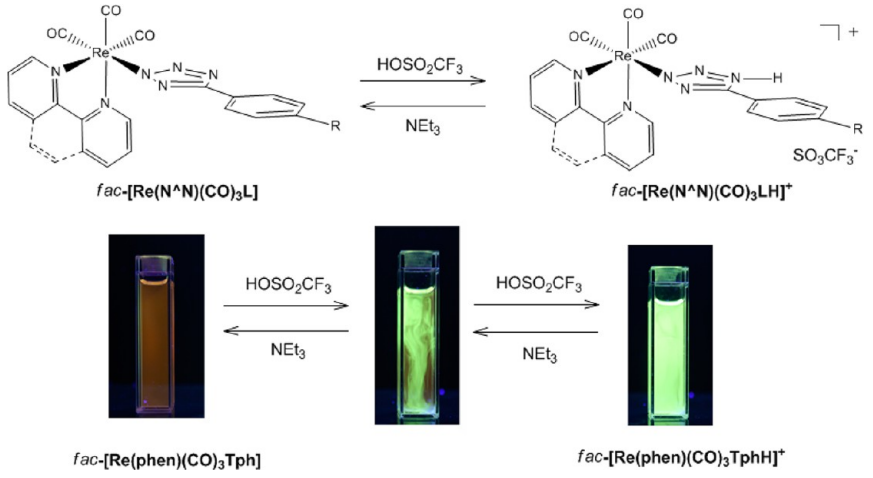

Figure 7. Protonation−deprotonation scheme (top) of *fac*-[Re(N^N)$(CO)_3$L]-type complexes and (bottom) images of the cuvettes containing the starting *fac*-[Re(phen)$(CO)_3$Tph] (left) the protonated *fac*-[Re(phen)$(CO)_3$TphH]$^+$ (right) and an the intermediate mixture of the two complexes (middle). λ_{exc} = 365 nm.

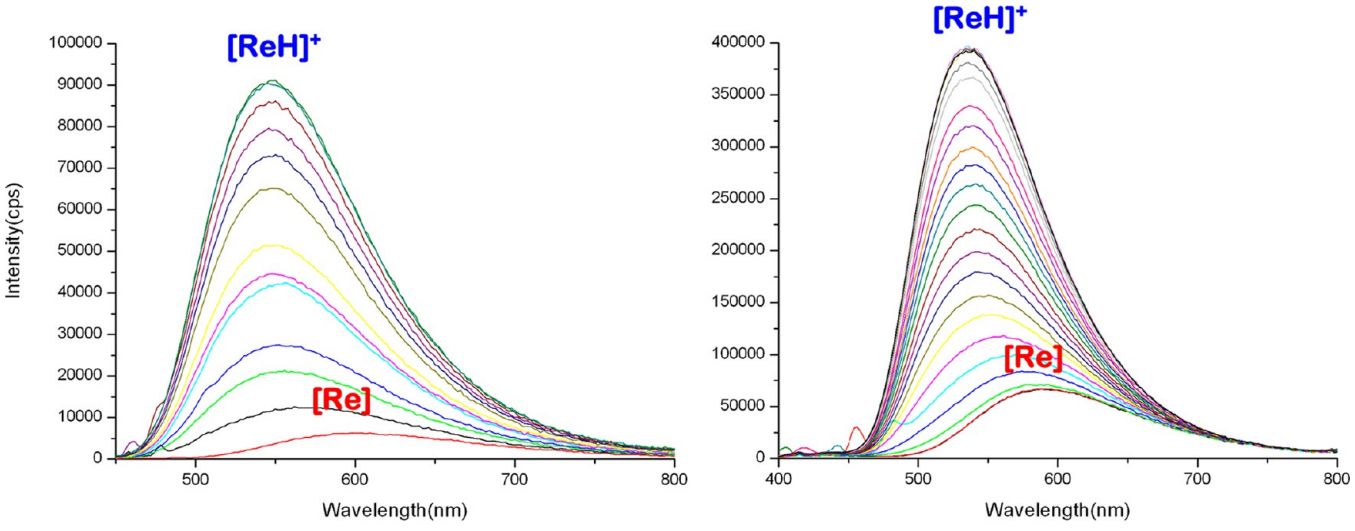

Figure 8. Steady-state emission spectra showing the blue shift and the increase of emission intensity occurring upon the transformation of *fac*-[Re(bpy)$(CO)_3$Tph] (left) and *fac*-[Re(phen)$(CO)_3$Tph] (right), denoted as [Re], into the corresponding protonated species, denoted as [ReH]$^+$.

a quite similar result is deduced from the interpretation of the time-resolved analysis, that again enlightens the elongation of lifetime fitting decays (τ) of the phosphorescent emissions on going from the neutral species (relative to air-equilibrated

dx.doi.org/10.1021/ic402187e | *Inorg. Chem.* 2014, 53, 229−243

samples, τ ranges from 85 to 107 ns for the bpy-containing complexes or from 268 to 382 ns for the phen-based ones) to the corresponding protonated complexes (τ of bpy complexes spans between 595 and 655 ns, whereas τ spans between 1.3 and 1.8 μs for the phen complexes). Again, the emissions that are displayed by the new protonated species are sensitive to the presence of oxygen, and their originating from an excited state with prevalent ^{3}MLCT character is suggested by the blue shift of the emission maxima that is observed from the same samples frozen at 77 K (Table 4 and Figures S14–S16, Supporting Information).

As might be expected for such reactions, the protonated compounds can be reconverted to the corresponding initial neutral complexes by treatment with a base, e.g., triethylamine (Figure 7). Importantly, such behavior introduces the possibility of reversibly modulating the luminescent features of neutral Re(I) tetrazolate complexes via a protonation–deprotonation regime.

These results prompted us to determine whether such a reversible modulation of the luminescence performances might be regarded as a general feature of luminescent metal tetrazolate complexes. To investigate the generality of this behavior, we first took into consideration the protonation of one of the cyclometalated Ir(III)-tetrazolate complexes that we have reported previously,[12a] namely, Ir(PyrTz); see Table 5, Figure 9, and Figure S17, Supporting Information.

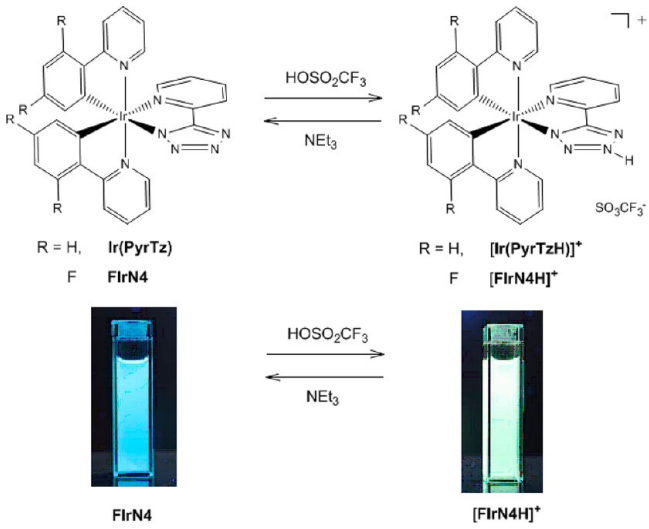

Figure 9. Protonation–deprotonation scheme (top) of Ir(III)-tetrazolate complexes and (bottom) images of the cuvettes containing the starting FIrN4 (left) and the protonated $[FIrN4H]^+$ (right). λ_{exc} = 365 nm.

As can be seen in Figures 9 and 10, the blue-green emitting Ir(III) tetrazolate neutral complex Ir(PyrTz) can be gradually transformed into the corresponding protonated species $[Ir(PyrTzH)]^+$, which displays an equally intense and red-shifted emission, following a trend that is quite similar to the one we previously observed for the methylation of the same complex.[12a] Again, the proton-induced modulation is fully reversible (Figure 9). An analogous effect is observed when performing the same protonation–deprotonation reactions onto the fluorinated Ir(III) tetrazolate complex that is usually denoted as FIrN4.[18] Also in this case, protonation red shifts the sky-blue emission of the latter species to the same extent as that reported for Ir(PyrTz), with the only difference being represented by the pronounced improvement of the quantum yield values of the couple FIrN4/$[FIrN4H]^+$ with respect to that observed in the cases of the nonfluorinated complexes Ir(PyrTz) and $[Ir(PyrTzH)]^+$ (Figure 10 and Table 5). It is important to note that, apart from the red shift of the emission, protonation likely causes significant changes in the nature of the emitting excited states of Ir(III) tetrazolate complexes. Upon protonation, the vibronically structured emission profiles of Ir(PyrTz) and FIrN4, which reflect the presence of closely spaced ^{3}LC and ^{3}MLCT emissive states, turn to broad and featureless emission spectra, which are more typical of pure CT states. This behavior might be explained in consideration of the reduction or total loss of the ^{3}LC contribution in the composition of the emitting excited states, which takes place on going from the neutral starting complex to the cationic product. In addition, the variation of the nature of the emitting excited states that occurs upon protonation of both Ir(PyrTz) and FIrN4 can be also experimentally deduced from the comparison of the emission profiles obtained at room temperature with those of the same complexes frozen at 77 K (Table 5 and Figures S19 and S20, Supporting Information). It is indeed possible to observe how the rigidochromic blue shift of the emission maxima, which is typical for MLCT-based excited states, was more evident for the cationic protonated complexes $[Ir(PyrTzH]^+$ and $[FIrN4H]^+$ (Figure S20, Supporting Information) than that observed in the cases of the corresponding neutral precursors (Figure S19, Supporting Information). However, these considerations are supported by computational calculations (*vide infra*), the results of which also indicate that the tetrazolate ligand is the main contributor to the LUMO-type orbitals of the protonated complex.

Finally, our investigation was completed with the analysis of the influence played by the protonation of a Ru(II)-based metal tetrazolate complex such as $[Ru(PyrTz)]^+$ (Table 5, Figure 11, and Figures S22 and S23, Supporting Information). As we reported earlier,[11e] this Ru(II) complex, when excited at 460 nm, displays a typically MLCT-shaped broad emission profile centered at λ_{max} = 653 nm. In sharp contrast with what we observed in the case of the methylation of the same substrate,[11e] this radiative process is completely quenched upon protonation (Figure 11). A similar behavior might be attributed to the occurrence in the protonated complex $[Ru(bpy)_2(PyrTzH)]^{2+}$ of thermally populated ^{3}MC excited states or, more likely, to the shift of the MLCT-centered emission toward the near-infrared (NIR) region, the presence of which cannot be detected, in agreement with the predictions of the energy gap law.[17] Unfortunately, by now it has not been possible to circumstantiate these attributions by means of TD-DFT calculations, whose results are not yet decisive. However, even though the reasons for such an apparently anomalous quenching phenomenon are not yet fully elucidated, it is important to note that, as a very important and common feature of all the other metal-tetrazolate complexes described herein, the emission of light from the Ru(II)-tetrazole complex $[Ru(bpy)_2(PyrTzH)]^{2+}$ can be experimentally restored upon its treatment with one molar equivalent of triethylamine, thereby leading to the re-formation of the starting Ru(II)-tetrazolate species $[Ru(bpy)_2(PyrTz)]^+$ (Figure 11).

TD-DFT Calculations. To further support the interpretation of the photophysical results, the energetics and absorption spectra of the complexes were simulated with time-dependent density functional theory using GAUSSIAN09.[19] It must be

dx.doi.org/10.1021/ic402187e | *Inorg. Chem.* 2014, 53, 229–243

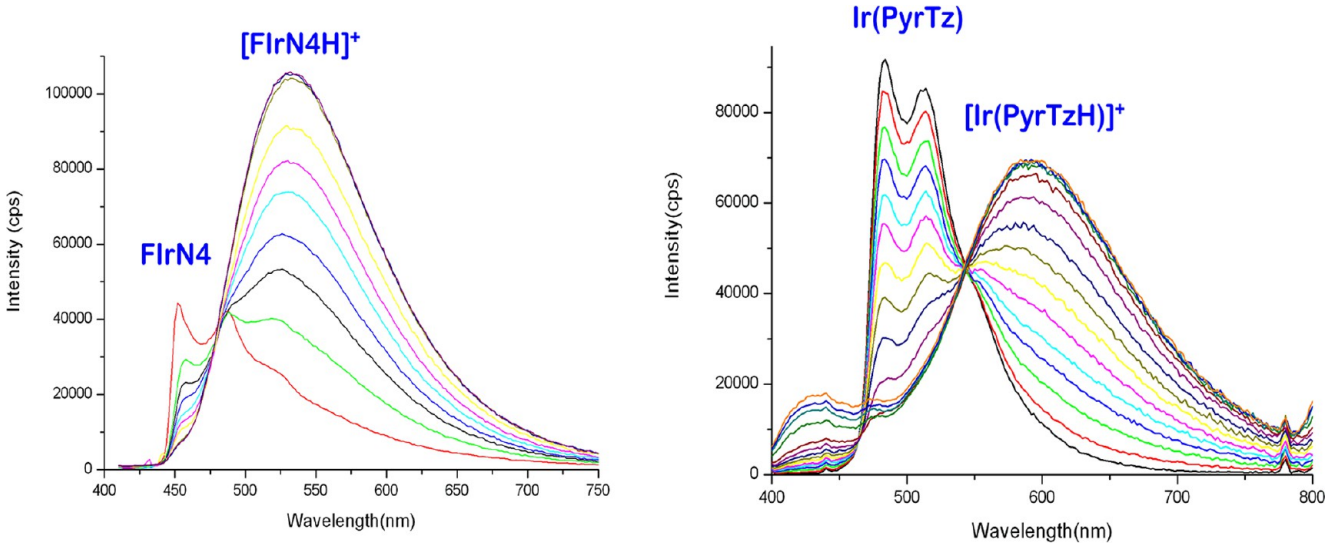

Figure 10. Steady-state emission spectra showing the changes in the emission profiles of FIrN4 (left) and Ir(PyrTz) (right) occurring upon their transformation to $[FIrN4H]^+$ and $[Ir(PyrTzH)]^+$, respectively.

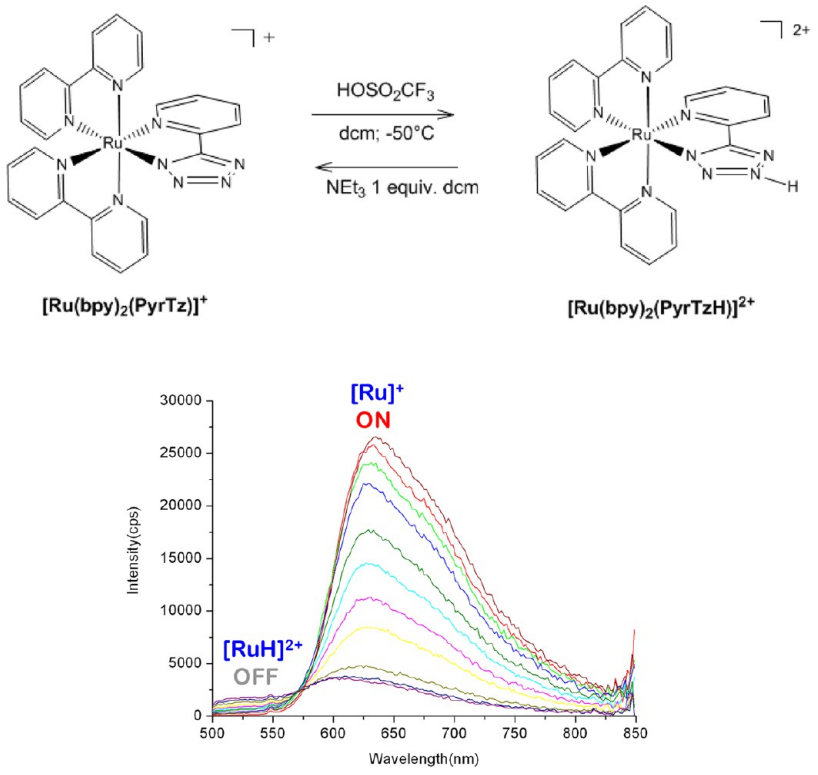

Figure 11. $[Ru(bpy)_2(PyrTz)]^+$: protonation−deprotonation procedure (top) and graphics showing the quenching of the emission occurring upon transformation of $[Ru(bpy)_2(PyrTz)]^+$, $[Ru]^+$, into the protonated $[Ru(bpy)_2(PyrTzH)]^{2+}$, $[RuH]^{2+}$, (bottom).

noted that for the *fac*-$[Re(bpy)(CO)_3TphH]^+$ complex, single crystals suitable for X-ray diffraction analysis could not be obtained. However, the TD-DFT calculations of this species were carried out by assuming that the protonation trend was the same as the other protonated Re(I) complexes, for which X-ray structures were available. According to our previous studies, the lowest energy excited states for the neutral rhenium complexes were characterized by an MLCT nature, partially mixed with LLCT character (MLLCT).[13a,b] For the protonated rhenium species investigated here, the lowest energy excited state seems to originate predominantly from HOMO−n → LUMO transitions, where n = 0−2 (Figures 12 and 13 and Supporting Information Figures S24−S35 and corresponding Tables S4−S9). Importantly, in this case, the contribution from the tetrazole π system in the HOMO−n orbitals is lost and they are exclusively composed of 5d orbitals of the Re center. On the other hand, as expected, the LUMO orbital is localized on the diimine ligand. Therefore, the lowest energy excited state is assigned to an MLCT process. The decrease in electron density experienced by the tetrazolate ring upon protonation indirectly causes the stabilization of the HOMO−n orbitals on the Re center. The high-energy transition seen in the absorption

dx.doi.org/10.1021/ic402187e | *Inorg. Chem.* 2014, 53, 229−243

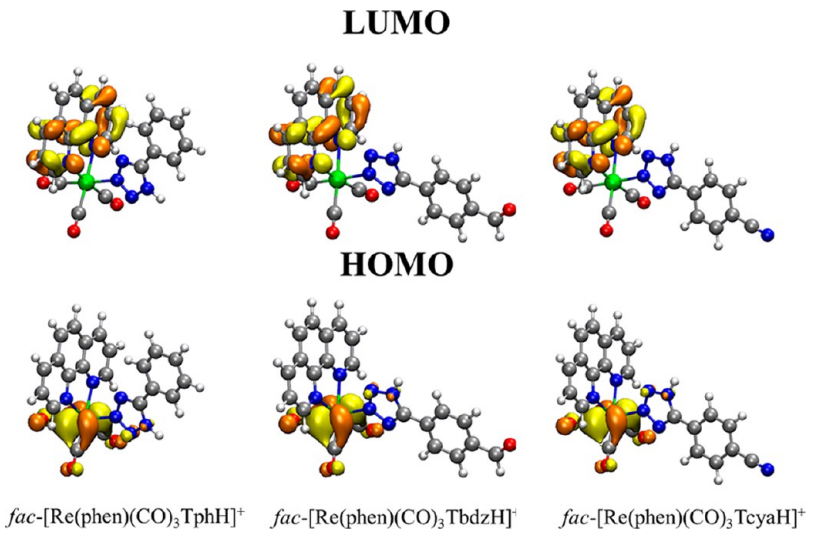

Figure 12. Localization of the HOMO and LUMO orbitals for the three *fac*-[Re(phen)$(CO)_3$LH]$^+$ complexes.

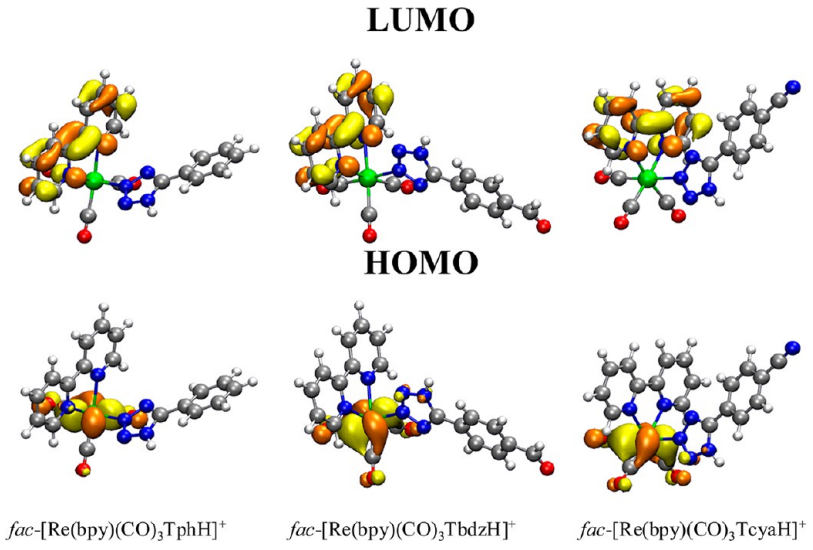

Figure 13. Localization of the HOMO and LUMO orbitals for the three *fac*-[Re(bpy)$(CO)_3$LH]$^+$ complexes.

spectra can be assigned to a mixture of LLCT and $\pi-\pi^*$ LC transitions.

The neutral Ir(PyrTz) has been calculated previously and supports the assignment of the lowest energy transitions possessing a mixture of ^{3}LC and ^{3}MLCT character.[12b] The lowest excited state for the protonated species [Ir(PyrTzH)]$^+$ appears to originate from predominantly HOMO → LUMO+m transitions, where m = 0−2 (Figure 14 and Supporting Information Figures S36−S37 and Table S10). This confirms that the lowest excited state is composed mainly of transitions of an MLCT and LLCT nature. There is also a small contribution from the LC, but this reduced contribution in comparison to the neutral analogue can explain the shift to a broad and structureless emission upon protonation. The lowest energy transitions for the FIrN4 complex appear to originate from HOMO → LUMO+m transitions, where m = 0−2 (Figure 14). This supports the assignment of the lowest excited state to be predominantly ^{3}MLCT and ^{3}LC in character, with a small contribution from LLCT. In the corresponding [FIrN4H]$^+$ complex, the lowest energy transitions appear to originate from primarily HOMO−n → LUMO+m transitions, where n = 0−1 and m = 0−3 (Figure 14 and Supporting Information Figures S38 and S39 and Table S11). This indicates that the lowest energy transitions possess mainly MLCT and LLCT character, with a significant reduction in the contribution from the LC transition. This again supports the transition from a structured emission from the neutral FIrN4 complex to a broad structureless emission upon protonation.

In order to provide a general picture of the behavior of these two classes of tetrazolate complexes, the energies of the frontier molecular orbitals for *fac*-[Re(phen)$(CO)_3$Tph] and $FIrN_4$ have been plotted along with their respective protonated complexes (Figure 15). In the case of the Re complex, it is apparent how the protonation of the tetrazole ring causes a strong stabilization of the HOMO orbital by indirectly reducing the electron density on the Re center. On the other hand, the LUMO localized on the phen ligand is only marginally affected. The orbital contours of the neutral and protonated complexes also highlight how the lowest excited state changes its character from MLLCT to MLCT upon protonation. In the case of the Ir complex, the tetrazole ring is directly involved in the composition of the LUMO orbital; hence the protonation

dx.doi.org/10.1021/ic402187e | *Inorg. Chem.* 2014, 53, 229−243

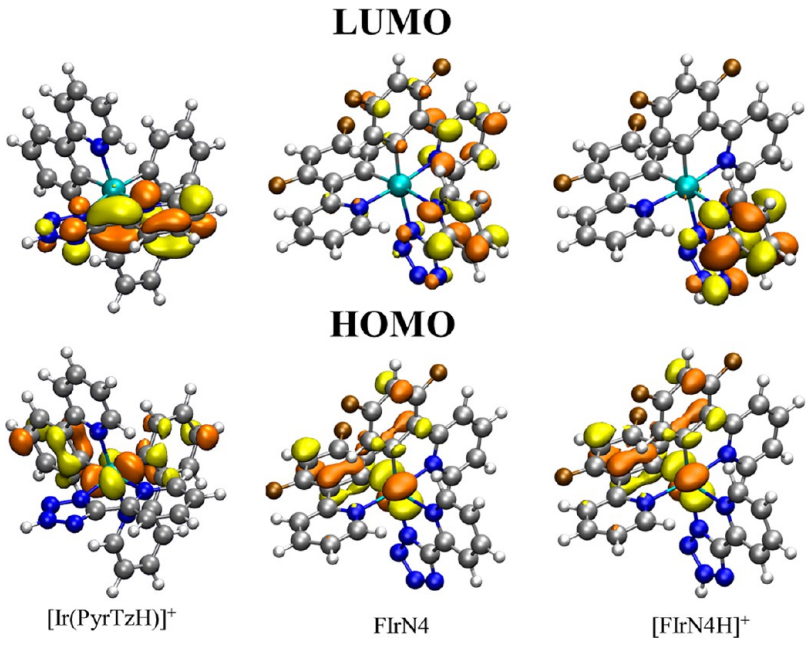

Figure 14. Localization of the HOMO and LUMO orbitals for the $[Ir(PyTzH)]^+$, FIrN4, and $[FIrN4H]^+$ complexes.

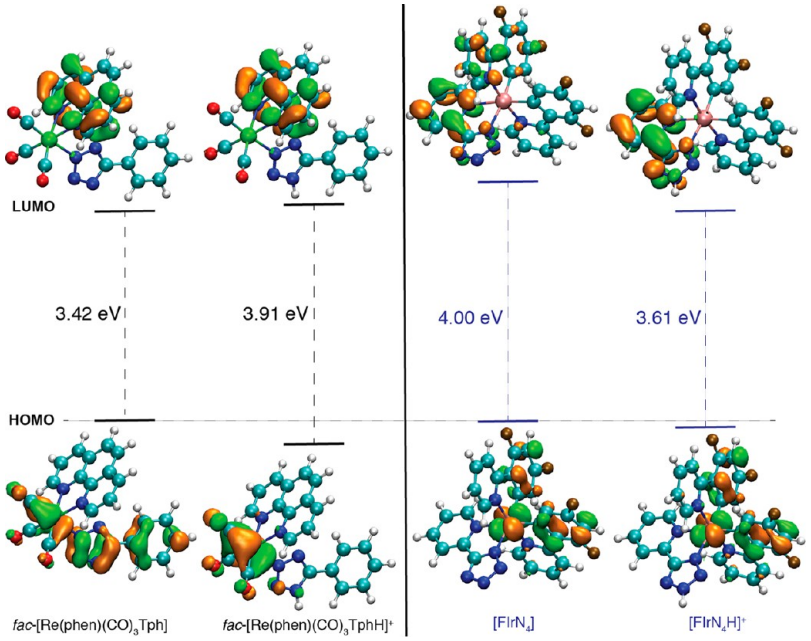

Figure 15. Calculated energy levels and orbital contours for the HOMO and LUMO orbitals of the *fac*-$[Re(phen)(CO)_3Tph]$ and $FIrN_4$ and their protonated versions obtained from the TD-DFT calculations. The energies of the Kohn–Sham HOMO orbitals for the nonprotonated and protonated complexes have been positioned by aligning the lowest energy orbitals that are not perturbed by the protonation.

causes its stabilization with consequent reduction in the HOMO–LUMO gap. As a consequence, the ligand-centered character of the excited state is lost, as it can be deduced from the analysis of the respective orbital contours.

CONCLUSIONS

Within the framework of our studies about the reactivity of metal tetrazolate complexes, we have investigated the proton-induced reversible modulation of the luminescence properties of *fac*-tricarbonyl diimine Re(I) tetrazolates. In particular, we have shown that by protonation reaction it was possible to blue shift and dramatically increase the intensity of light emission from neutral Re(I) tetrazolate complexes as the result of their conversion into the corresponding protonated cationic derivatives. This perturbation, which might be properly described as a "luminescence boosting reaction", can be efficiently removed by the addition of a base to the protonated complexes, taking the system back to the initial stage. A quite similar variation of the luminescent performances, even if to a less "dramatic" extent, occurs in the case of Ir(III) tetrazolate complexes, the luminescence features of which can be again reversibly modulated by the means of the same protonation–deprotonation mechanism. Interestingly, the luminescence modulation of these Ir(III) complexes is not just a matter of

dx.doi.org/10.1021/ic402187e | *Inorg. Chem.* 2014, 53, 229–243

shifting the emission color and/or varying the intensity of the radiative processes, but it involves also the substantial change of the nature of the emitting excited states, which reversibly passes from closely spaced ^{3}LC/^{3}MLCT combination (neutral species) to an admixture of ^{3}MLCT and ^{3}LLCT-type excited states (as for the protonated complexes). Yet a different behavior is displayed by a polypyridyl Ru(II) tetrazolate complex such as $[Ru(bpy)_2L]^+$, for which the application of the protonation−deprotonation reaction's protocol causes the reversible ON−OFF switching of the emissive performances. In all cases, the presence of such pronounced electrophile sensitivity reflects the important role played by the tetrazolate ligands in determining the extent of the HOMO−LUMO gap. In general, these findings might be quite important for further widening the application perspectives of metal tetrazolate complexes. Indeed, the chance of modulating the emission color in connection with the variation of the charge of the complexes involves the presence of species that likely display different solubility in aqueous solvents. If the color change would occur in a biologically useful pH range (6−8), both Ir(III) and, particularly, Re(I) tetrazolate complexes might have all the characteristics for behaving as imaging and/or sensing agents. In this context, studies about the influence of pH on the luminescence behavior and the efficiency of cell uptake of luminescent metal tetrazolate complexes are currently being undertaken.

EXPERIMENTAL SECTION

General Considerations. All the reagents and solvents were obtained commercially (e.g., Aldrich) and used as received without any further purification, unless otherwise specified. The preparation of the starting Ir(III) complexes, namely, Ir(PyrTz)[12a] and FIrN4,[16] and the Ru(II) species $[Ru(PyrTz)][PF_6]$[11e] was accomplished by following methods reported in the literature. All the reactions were carried out under an argon atmosphere following Schlenk protocols. Where required, the purification of the Re complexes was performed via column chromatography with the use of neutral alumina as the stationary phase. ESI-mass spectra were recorded using a Waters ZQ-4000 instrument (ESI-MS, acetonitrile as the solvent). IR spectra were recorded as dichloromethane (DCM) solutions, using a NaCl (5 mm) disc on a Perkin-Elmer Spectrum 2000 FT-IR spectrometer. Nuclear magnetic resonance spectra (consisting of ^{1}H and ^{13}C experiments) were always recorded using a Varian Mercury Plus 400 instrument (^{1}H, 400.1; ^{13}C, 101.0 MHz) at room temperature. ^{1}H and ^{13}C chemical shifts were referenced to residual solvent resonances. With the exception of the new complex *fac*-$[Re(bpy)(CO)_3Tcya]$, the spectroscopic data of the neutral Re(I) complexes *fac*-$[Re(N^\wedge N)(CO)_3L]$, where N^N is bpy or phen, L = Tph, Tbdz,[13a] and *fac*-$[Re(phen)(CO)_3Tcya]$,[13c] have been described previously. However, for comparison purpose, their ESI-MS, IR, and NMR data have also been reported herein. It has to be noted that the analysis of the ^{1}H NMR spectra of the protonated Re(I) complexes indicates the presence of tiny but detectable amounts of decomposition byproducts (see Supporting Information, Figures S2−S7), which likely derive from tetrazole displacement processes that could be likely promoted by the addition of a slight excess of triflic acid to the complexes prior to the preparation of the samples. However, the contamination of the desired product was never found to be higher than ca. 8−10% (as in the batches containing the complexes *fac*-$[Re(N^\wedge N)(CO)_3TphH]^+$; see Supporting Information, Figures S6 and S7).

Relative to the description of the ^{1}H NMR spectra (see further on), the atom numbering always refers to Scheme 2.

Photophysics. Absorption spectra were recorded at room temperature using a Perkin-Elmer Lambda 35 UV/vis spectrometer. Uncorrected steady-state emission and excitation spectra were recorded on an Edinburgh FLSP920 spectrometer equipped with a 450 W xenon arc lamp, double excitation and single emission monochromators, and a Peltier-cooled Hamamatsu R928P photomultiplier tube (185−850 nm). Emission and excitation spectra were corrected for source intensity (lamp and grating) and emission spectral response (detector and grating) by a calibration curve supplied with the instrument. The wavelengths for the emission and excitation spectra were determined using the absorption maxima of the metal-to-ligand charge transfer (MLCT) transition bands (emission spectra) and at the maxima of the emission bands (excitation spectra). According to the approach described by Demas and Crosby,[20] luminescence quantum yields (Φ_{em}) were measured in optically dilute solutions (OD < 0.1 at excitation wavelength) obtained from absorption spectra on a wavelength scale [nm] and compared to the reference emitter by the following equation:[21]

$$\Phi_x = \Phi_r\left[\frac{A_r(\lambda_r)}{A_x(\lambda_x)}\right]\left[\frac{I_r(\lambda_r)}{I_x(\lambda_x)}\right]\left[\frac{n_x^2}{n_r^2}\right]\left[\frac{D_x}{D_r}\right]$$

where A is the absorbance at the excitation wavelength (λ), I is the intensity of the excitation light at the excitation wavelength (λ), n is the refractive index of the solvent, D is the integrated intensity of the luminescence, and Φ is the quantum yield. The subscripts r and x refer to the reference and the sample, respectively. The quantum yield determinations were performed at identical excitation wavelengths for the sample and the reference, therefore canceling the $I(\lambda_r)/I(\lambda_x)$ term in the equation. All the Re(I) complexes were measured against an ethanol solution of rhodamine 101 used as reference ($\Phi_r = 1$),[22] while quinine bisulfate in 1.0 N sulfuric acid was used as reference ($\Phi_r = 0.546$)[23] for the Ir(III) complexes. Emission lifetimes (τ) were determined with the single photon counting technique (TCSPC) with the same Edinburgh FLSP920 spectrometer using pulsed picosecond LEDs (EPLED 295 or EPLED 360, fhwm <800 ps) as the excitation source, with repetition rates between 1 kHz and 1 MHz, and the above-mentioned R928P PMT as detector. The goodness of fit was assessed by minimizing the reduced χ^2 function and by visual inspection of the weighted residuals. To record the 77 K luminescence spectra, the samples were put in quartz tubes (2 mm diameter) and inserted in a special quartz dewar filled with liquid nitrogen. The solvent (dichloromethane) used in the preparation of the solutions for the photophysical investigations was of spectrometric grade. Degassed solutions were prepared by gently bubbling argon gas into the prepared sample for 15 min before measurement. Experimental uncertainties are estimated to be ±8% for lifetime determinations, ±20% for quantum yields, and ±2 and ±5 nm for absorption and emission peaks, respectively.

COMPUTATIONAL CALCULATIONS

The TD-DFT calculations were performed using the B3LYP functional,[24] the Stuttgart-Dresden effective core potential for Re,[25] and the 6-311++G** basis set for the other atoms. The presence of the solvent was then mimicked by using the PCM implicit solvation model[26] with parameters appropriate for dichloromethane.

Synthesis. ***Warning!*** *Tetrazole derivatives are used as components for explosive mixtures.*[16] In this lab, the reactions described here were only run on a few grams' scale and no problems were encountered. However, great caution should be exercised when handling or heating compounds of this type.

The formation of the tetrazolate anions $[Tph]^-$, $[Tcya]^-$, and $[Tbdz]^-$ was achieved by the addition of equimolar amounts of triethylamine to a suspension of the neutral 5-substituted tetrazoles in absolute ethanol (5 mL). The resulting pale yellow solutions were used without any further purification.

General Procedure for the Preparation of the Neutral *fac*-[Re(N^N)(CO)$_3$L]-Type Complexes. A 0.100 g amount of *fac*-$[Re(\hat{N}N)(CO)_3Br]$ (0.20 mmol for N^N = bpy; 0.19 mmol if N^N = phen) was dissolved in 20 mL of an ethanol/water mixture (3:1 v/v) under an argon atmosphere. A 5.0 mL portion of an ethanol/water (3:1 v/v) solution containing 1.5 equiv of the appropriate tetrazolate salt was added dropwise. Once the addition was completed, the resulting suspension was stirred at the reflux temperature for 20 h. After this time, the mixture was cooled to rt and filtered through a

dx.doi.org/10.1021/ic402187e | Inorg. Chem. 2014, 53, 229−243

glass frit, affording the desired complexes as a yellow microcrystalline powder. In most cases, the product complexes did not require any further purification process, the exceptions being *fac*-[Re(bpy)-$(CO)_3$Tbdz] and *fac*-[Re(phen)$(CO)_3$Tcya]. These latter compounds were obtained as the second fractions upon performing alumina-filled column chromatographies using acetonitrile as the eluent.

fac-[Re(bpy)(CO)$_3$Tph]. Yield: 0.072 g, 63%. ESI-MS (m/z) = 595 $[M + Na]^+$. IR (ν, cm^{-1}, CH_2Cl_2, rt): 2029 s (CO, A′(1)), 1924 s br (CO, A′(2)/A″), 1606 w (tetrazole C═N). ^{1}H NMR (δ, ppm, acetone-d_6): 9.25 (2H, d, J = 5.2 Hz, $H_{2,2'}$), 8.69 (2H, d, J = 8.0 Hz, $H_{5,5'}$), 8.35 (2H, t, J = 7.2 Hz, $H_{4,4'}$), 7.82−7.79 (4H, m, $H_{3,3'}$ and H_{ortho}), 7.32−7.24 (3H, m, H_{meta} and H_{para}). ^{13}C NMR (δ, ppm, acetone-d_6): 163.7, 157.5, 154.7, 141.2, 131.5, 129.2, 128.9, 128.7, 126.8, 124.7.

fac-[Re(phen)(CO)$_3$Tph]. Yield: 0.085 g, 75%. ESI-MS (m/z) = 619 $[M + Na]^+$. IR (ν, cm^{-1}, CH_2Cl_2, rt): 2029 s (CO, A′(1)), 1922 s br (CO, A′(2)/A″), 1606 w (tetrazole CN). ^{1}H NMR (δ, ppm, acetone-d_6): 9.65 (2H, d, J = 4.8 Hz, $H_{2,2'}$), 8.96 (2H, d, J = 8.2 Hz, $H_{4,4'}$), 8.30 (2H, s, $H_{5,5'}$), 8.19−8.15 (2H, m, $H_{3,3'}$), 7.63 (2H, d, J = 7.2 Hz, H_{ortho}), 7.22−7.20 (3H, m, 2H_{meta} and H_{para}). ^{13}C NMR (δ, ppm, acetone-d_6): 163.4, 155.1, 148.3, 140.3, 131.7, 131.3, 129.1, 128.9, 128.7, 127.4, 126.6.

fac-[Re(bpy)(CO)$_3$Tbdz]. The complex was purified via alumina-filled column chromatography using a 100% acetonitrile solvent system as eluent (second fraction, yellow). Yield: 0.067 g, 56%. ESI-MS (m/z) = 623 $[M + Na]^+$. IR (ν, cm^{-1}, CH_2Cl_2, rt): 2029 s (CO, A′(1)), 1922 br (CO, A′(2)/A″), 1699 s (aldehyde CO), 1607 w (tetrazole C═N). ^{1}H NMR (δ, ppm, acetone-d_6): 10.01 (1H, s, −C*H*O), 9.27 (2H, d, J = 5.5 Hz, $H_{2,2'}$), 8.71 (2H, d, J = 8.4 Hz, $H_{5,5'}$), 8.37 (2H, t, J = 7.8 Hz, $H_{4,4'}$), 8.01 (2H, d, J = 8.0 Hz, H_{ortho}), 7.87 (2H, d, J = 8.4 Hz, H_{meta}), 7.83 (2H, t, J = 5.6 Hz, $H_{3,3'}$). ^{13}C NMR (δ, ppm, acetone-d_6): 192.4, 163.0, 157.5, 154.7, 141.3, 137.2, 136.7, 130.6, 128.7, 127.1, 124.7.

fac-[Re(phen)(CO)$_3$Tbdz]. Yield: 0.097g, 82%. ESI-MS (m/z) = 647 $[M + Na^+]$. IR (ν, cm^{-1}, CH_2Cl_2, rt): 2029 s (CO, A′(1)), 1923 br (CO, A′(2)/A″), 1699 s (aldehyde CO), 1610 w (tetrazole C═N). ^{1}H NMR (δ, ppm, acetone-d_6): 9.96 (1H, s, −C*H*O), 9.67 (2H, d, J = 5.2 Hz, $H_{2,2'}$), 8.98 (2H, d, J = 8.4 Hz, $H_{4,4'}$), 8.32 (2H, s, $H_{5,5'}$), 8.20−8.17 (2H, m, $H_{3,3'}$), 7.84 (2H, d, J = 8.8 Hz, H_{meta}), 7.80 (2H, d, J = 8.4 Hz, H_{ortho}). ^{13}C NMR (δ, ppm, acetone-d_6): 192.4, 162.8, 155.2, 148.2, 140.4, 137.1, 136.6, 131.7, 130.5, 128.7, 127.4, 127.0.

fac-[Re(bpy)(CO)$_3$Tcya]. Yield: 0.090 g, 75%). ESI-MS (m/z) = 620 $[M + Na^+]$. IR (ν, cm^{-1}, CH_2Cl_2, rt): 2229 w (CN), 2029 s (CO, A′(1)), 1923 br (CO, A′(2)/A″), 1606 w (tetrazole C═N). ^{1}H NMR (δ, ppm, acetone-d_6): 9.27 (2H, d, J = 5.5 Hz, $H_{2,2'}$), 8.71 (2H, d, J = 8.40 Hz, $H_{5,5'}$), 8.37 (2H, t, J = 8 Hz, $H_{4,4'}$), 7.96 (2H, d, J = 9.2 Hz, H_{ortho}), 7.83−7.79 (2H, m, $H_{3,3'}$), 7.72 (2H, d, J = 7.5 Hz, H_{meta}). ^{13}C NMR (δ, ppm, acetone-d_6): 162.5, 157.4, 154.7, 141.3, 135.5, 133.3, 128.7, 127.3, 124.7, 119.3, 112.3. Crystals suitable for X-ray analysis (identified as *fac*-[Re(bpy)$(CO)_3$(Tcya)], $C_{21}H_{12}N_7O_3Re$) were obtained by slow diffusion of diethyl ether into a solution of the complex in dichloromethane. Anal. Calcd for $C_{21}H_{12}N_7O_3Re$ (596.570): C, 42.28; H, 2.03; N, 16.43. Found: C, 42.25; H, 1.88; N, 16.26.

fac-[Re(phen)(CO)$_3$Tcya]. The complex was purified via alumina-filled column chromatography using pure acetonitrile as the eluent (second fraction, yellow). Yield: 0.050 g, 42%. ESI-MS (m/z) = 644 $[M + Na^+]$. IR (ν, cm^{-1}, CH_2Cl_2, rt): 2229 w (CN), 2030 s (CO, A′(1)), 1923 br (CO, A′(2)/A″), 1606 w (tetrazole C═N). ^{1}H NMR (δ, ppm, acetone-d_6): 9.67 (2H, d, J = 4.0 Hz, $H_{2,2'}$), 8.97 (2H, d, J = 7.2 Hz, $H_{4,4'}$), 8.31 (2H, s, $H_{5,5'}$), 8.20−8.16 (2H, m, $H_{3,3'}$), 7.81 (2H, d, J = 6.4 Hz, H_{ortho}), 7.65 (2H, d, J = 4.0 Hz, H_{meta}). ^{13}C NMR (δ, ppm, acetone-d_6): 162.4, 155.2, 148.2, 140.4, 135.3, 133.2, 131.7, 128.7, 127.4, 127.1, 119.3, 112.2.

General Procedure for the Protonation of Re(I), Ir(III), and Ru(II) Tetrazolate Complexes. In a typical procedure,[27] 0.050 g of the appropriate Re(I), Ir(III), or Ru(II) metal tetrazolate precursor was dissolved in 15 mL of dichloromethane. The resulting solution was cooled to −50 °C, and an excess (1.5 equiv) of $HOSO_2CF_3$ (0.124 M solution in dichloromethane) was added. After being maintained at −50 °C for 30 min, the mixture was left to stir overnight at rt. The solvent was then removed by rotary evaporation, affording generally oily yellow, i.e., Re(I) and Ir(III), or red, as for Ru(II), residues that were identified as the expected protonated complexes.

fac-[Re(phen)(CO)$_3$TphH][SO$_3$CF$_3$]. Yield: 0.051 g, 82%. ESI-MS (m/z) = 597 $[M - SO_3CF_3]^+$; 149 $[SO_3CF_3]^-$. IR (ν, cm^{-1}, CH_2Cl_2, rt): 2039 s (CO, A′(1)), 1936 br (CO, A′(2)/A″), 1606 w (tetrazole C═N). ^{1}H NMR (δ, ppm, acetone-d_6): 9.75 (2H, d, J = 4.8 Hz, $H_{2,2'}$), 9.07 (2H, d, J = 8.0 Hz, $H_{4,4'}$), 8.37 (2H, s, phen $H_{5,5'}$), 8.28−8.24 (2H, m, phen $H_{3,3'}$), 7.69 (2H, d, J = 7.6 Hz, H_{ortho}), 7.56−7.54 (1H, m, H_{para}), 7.43−7.39 (2H, m, H_{meta}). ^{13}C NMR (δ, ppm, acetone-d_6): 197.0, 156.4, 156.2, 148.8, 141.8, 134.1, 132.7, 131.0, 129.6, 128.8, 128.5. Crystals suitable for X-ray analysis were obtained by slow diffusion of diethyl ether into a solution of the complex in dichloromethane and a few drops of dilute triflic acid solution. By using this procedure, two different crystals of the same complex were obtained—*fac*-[Re(phen)$(CO)_3$TphH][CF_3SO_3], $C_{23}H_{14}F_3N_6O_6ReS$, and *fac*-[Re(phen)$(CO)_3$TphH][CF_3SO_3]·0.25Et_2O, $C_{24}H_{16.5}F_3N_6O_{6.25}ReS$, respectively—which are distinguished by the presence of diethyl ether in the unit cell. Anal. Calcd for $C_{23}H_{14}F_3N_6O_6ReS$ (745.660): C, 37.04; H, 1.89; N, 11.27. Found: C, 37.15; H, 1.80; N. 11.09.

fac-[Re(bpy)(CO)$_3$TphH][SO$_3$CF$_3$]. Yield: 0.045 g, 70%. ESI-MS (m/z) = 573 $[M - SO_3CF_3]^+$; 149 $[SO_3CF_3]^-$. IR (ν, cm^{-1}, CH_2Cl_2, rt): 2039 s (CO, A′(1)), 1936 br (CO, A′(2)/A″), 1606 w (tetrazole C═N). ^{1}H NMR (δ, ppm, acetone-d_6): 9.31 (2H, d, J = 5.2 $H_{6,6'}$), 8.78 (2H, d, J = 8.4 Hz $H_{3,3'}$), 8.43−8.39 (2H, m, $H_{4,4'}$), 7.90−7.83 (4H, m, $H_{5,5'}$ and H_{ortho}), 7.54−7.49 (3H, m, H_{meta} and H_{para}). ^{13}C NMR (δ, ppm, acetone-d_6): 196.8, 194.3, 159.2, 157.5, 155.0, 141.9, 132.4, 130.1, 129.1, 127.9, 125.4, 123.3. Anal. Calcd for $C_{21}H_{14}F_3N_6O_6ReS$ (721.640): C, 34.95; H, 1.96; N, 11.64. Found: C, 35.20; H, 2.09; N, 11.77.

fac-[Re(phen)(CO)$_3$TbdzH][SO$_3$CF$_3$]. Yield: 0.042 g, 68%. ESI-MS (m/z) = 625 $[M - SO_3CF_3]^+$; 149 $[SO_3CF_3]^-$. IR (ν, cm^{-1}, CH_2Cl_2, rt): 2040 s (CO, A′(1)), 1938 br (CO, A′(2)/A″), 1709 s (aldehyde CO), 1607 w (tetrazole C═N). ^{1}H NMR (δ, ppm, acetone-d_6): 10.04 (1H, s, −C*H*O), 9.74 (2H, d, J = 5.2 Hz, $H_{2,2'}$), 9.04 (2H, d, J = 8.2 Hz, $H_{4,4'}$), 8.36 (2H, s, $H_{5,5'}$), 8.26−8.23 (2H, m, $H_{3,3'}$), 7.95 (2H, d, J = 8.4 Hz, H_{ortho}), 7.90 (2H, d, J = 8.4 Hz, H_{meta}). ^{13}C NMR (δ, ppm, acetone-d_6): 192.3, 155.7, 148.2, 141.0, 139.3, 132.0, 130.9, 128.9, 128.5, 127.7. Crystals suitable for X-ray analysis (identified as *fac*-[Re(phen)$(CO)_3$TbdzH][CF_3SO_3], $C_{24}H_{14}F_3N_6O_7ReS$) were obtained by slow diffusion of diethyl ether into a solution of the complex in dichloromethane and a few drops of dilute triflic acid solution. Anal. Calcd for $C_{24}H_{14}F_3N_6O_7ReS$ (773.670): C, 37.26; H, 1.82; N, 10.86. Found: C, 37.33; H, 1.90; N, 11.12.

fac-[Re(bpy)(CO)$_3$TbdzH][SO$_3$CF$_3$]. Yield: 0.035g, 56%. ESI-MS (m/z) = 601 $[M - SO_3CF_3]^+$; 149 $[SO_3CF_3]^-$. IR (ν, cm^{-1}, CH_2Cl_2, rt): 2040 s (CO, A′(1)), 1937 br (CO, A′(2)/A″), 1709 s (aldehyde CO), 1606 w (tetrazole C═N). ^{1}H NMR (δ, ppm, acetone-d_6): 10.11 (1H, s, −C*H*O), 9.34 (2H, d, J = 5.6 Hz, $H_{6,6'}$), 8.81 (2H, d, J = 8.2 Hz, $H_{3,3'}$), 8.45−8.43 (2H, m, $H_{4,4'}$), 8.07 (4H, s, H_{ortho} and H_{meta}), 7.91−7.88 (2H, *m*, $H_{5,5'}$). ^{13}C NMR (δ, ppm, acetone-d_6): 196.4, 192.4, 157.5, 155.1, 154.9, 142.4, 142.1, 139.9, 131.0, 129.2, 129.0, 125.3. Crystals suitable for X-ray analysis (identified as *fac*-[Re(bpy)$(CO)_3$TbdzH][CF_3SO_3], $C_{22}H_{14}F_3N_6O_7ReS$) were obtained by slow diffusion of diethyl ether into a solution of the complex in dichloromethane and a few drops of dilute triflic acid solution. Anal. Calcd for $C_{22}H_{14}F_3N_6O_7ReS$ (749.651): C, 35.25; H, 1.88; N, 11.21. Found: C, 35.31; H, 1.92; N 11.30.

fac-[Re(phen)(CO)$_3$TcyaH][SO$_3$CF$_3$]. Yield: 0.039 g, 64%. ESI-MS (m/z) = 622 $[M - SO_3CF_3]^+$; 149 $[SO_3CF_3]^-$. IR (ν, cm^{-1}, CH_2Cl_2, rt): 2233 w (CN), 2040 s (CO, A′(1)), 1937 br (CO, A′(2)/A″), 1606 w (tetrazole C═N). ^{1}H NMR (δ, ppm, acetone-d_6): 9.76 (2H, d, J = 5 Hz, $H_{2,2'}$), 9.07 (2H, d, J = 8.4 Hz, $H_{4,4'}$), 8.37 (2H, s, $H_{5,5'}$), 8.28−8.25 (2H, m, $H_{3,3'}$), 7.91 (4H, s, H_{meta} and H_{ortho}). ^{13}C NMR (δ, ppm, acetone-d_6): 196.3, 155.8, 148.1, 141.2, 134.1, 132.0, 129.0, 128.9, 127.8, 127.6, 126.8, 118.3, 116.5. Crystals suitable for X-ray analysis (identified as *fac*-[Re(phen)$(CO)_3$TcyaH][CF_3SO_3], $C_{24}H_{13}F_3N_7O_6ReS$) were obtained by slow diffusion of diethyl ether

dx.doi.org/10.1021/ic402187e | *Inorg. Chem.* 2014, 53, 229−243

into a solution of the complex in dichloromethane and a few drops of dilute triflic acid solution. Anal. Calcd for $C_{24}H_{13}F_3N_7O_6ReS$ (770.672): C, 37.40; H, 1.70; N, 12.72. Found: C, 37.33; H, 1.63; N, 12.42.

fac-[Re(bpy)(CO)$_3$TcyaH][SO$_3$CF$_3$]. Yield: 0.026 g, 42%. ESI-MS (m/z) = 598 $[M - SO_3CF_3]^+$; 149 $[SO_3CF_3]^-$. IR (ν, cm^{-1}, CH_2Cl_2, rt): 2233 w (CN), 2040 s (CO, A′(1)), 1938 br (CO, A′(2)/A″), 1606 w (tetrazole C═N). ^{1}H NMR (δ, ppm, acetone-d_6): 9.32 (2H, d, J = 5.4 Hz, $H_{6,6'}$), 8.78 (2H, d, J = 8.4 Hz, $H_{3,3'}$), 8.44 (2H, t, J = 8 Hz, $H_{4,4'}$), 8.04 (2H, d, J = 8.8 Hz, H_{ortho}), 7.94−7.88 (4H, m, H_{meta} and bpy $H_{5,5'}$). ^{13}C NMR (δ, ppm, acetone-d_6): 157.5, 154.9, 154.1, 141.7, 140.7, 133.7, 129.0, 128.2, 125.0, 118.8, 114.5. Crystals suitable for X-ray analysis (identified as *fac*-[Re(bpy)(CO)$_3$TcyaH][CF$_3$SO$_3$], $C_{22}H_{13}F_3N_7O_6ReS$) were obtained by slow diffusion of diethyl ether into a solution of the complex in dichloromethane. Anal. Calcd for $C_{24}H_{13}F_3N_7O_6ReS$ (746.650): C, 35.39; H, 1.75; N, 13.13. Found: C, 35.31; H, 1.90; N, 13.22.

[FIrN4H][SO$_3$CF$_3$]. Yield: 0.048 g, 80%). ESI-MS (m/z) = 719 $[M - SO_3CF_3]^+$; 149 $[SO_3CF_3]^-$. ^{1}H NMR (δ, ppm, acetonitrile-d_3): 8.49 (1H, d, J = 7.6 Hz), 8.12−8.24 (3H, m), 8.01 (1H, d, J = 5.2 Hz), 7.92 (2H, t, J = 7.6 Hz), 7.74 (1H, d, J = 5.6 Hz), 7.66−7.59 (2H, m), 7.13−7.07 (2H, m), 6.72−6.65 (2H, m), 5.75−5.71 (2H, m). Anal. Calcd for $C_{29}H_{17}F_7N_7O_3SIr$ (868.762): C, 40.09; H, 1.97; N, 11.28. Found: C, 40.20; H, 2.09; N, 11.39.

[Ir(PyrTzH)][SO$_3$CF$_3$]. Yield: 0.052 g, 85%. ESI-MS (m/z) = 648 $[M - SO_3CF_3]^+$; 149 $[SO_3CF_3]^-$. ^{1}H NMR (δ, ppm, acetonitrile-d_3): 8.33 (1H, d, J = 7.6 Hz), 8.02−7.99 (3H, m), 7.80−7.72 (5H, m) 7.61 (1H, d, J = 4.8 Hz), 7.55 (1H, d, J = 4.8 Hz), 7.32−7.29 (1H, m), 7.01−6.87 (5H, m), 6.83−6.79 (1H, m), 6.33 (1H, d, J = 7.6 Hz), 6.28 (1H, d, J = 7.6 Hz). Anal. Calcd for $C_{29}H_{21}F_3N_7O_3SIr$ (796.800): C, 43.71; H, 2.65; N, 12.30. Found: C, 43.65; H, 2.60; N, 12.60.

[Ru(bpy)$_2$(PyrTzH)][SO$_3$CF$_3$]$_2$. Yield: 0.045 g, 75%. ESI-MS: (m/z) 280 $[M]^{2+}$; 145 $[PF_6]^-$, 149 $[SO_3CF_3]^-$. ^{1}H NMR (CD_3CN, 400 MHz): 8.49 (2H, t, J = 7.2 Hz), 8.44−8.41 (2H, m), 8.35 (1H, d, J = 7.6 Hz), 8.05−7.94 (5H, m), 7.87−7.83 (2H, m), 7.79 (1H, d, J = 5.6 Hz), 7.69 (1H, d, J = 5.2 Hz), 7.62 (1H, d, J = 5.2 Hz), 7.41−7.29 (5H, m) ppm. An accurate determination of the bulk composition by elemental analysis could not be obtained due to the uncertain nature of the anionic counterpart, which is likely formed by one triflate ($CF_3SO_3^-$) and one hexafluorophosphate (PF_6^-) ion, as can be observed in the negative ion ESI-MS spectrum reported in Supporting Information, Figure S23.

X-ray Crystallography. Crystal data and collection details for *fac*-[Re(bpy)(CO)$_3$Tcya], *fac*-[Re(phen)(CO)$_3$TphH][CF$_3$SO$_3$], *fac*-[Re(phen)(CO)$_3$TphH][CF$_3$SO$_3$]·0.25Et$_2$O, *fac*-[Re(phen)(CO)$_3$TcyaH][CF$_3$SO$_3$], *fac*-[Re(phen)(CO)$_3$TbdzH][CF$_3$SO$_3$], *fac*-[Re(bpy)(CO)$_3$TcyaH][CF$_3$SO$_3$], and *fac*-[Re(bpy)(CO)$_3$TbdzH][CF$_3$SO$_3$] are reported in Tables S2 and S3 (Supporting Information). The diffraction experiments were carried out on a Bruker APEX II diffractometer equipped with a CCD detector and using Mo Kα radiation, except *fac*-[Re(bpy)(CO)$_3$Tcya], for which an Oxford Diffraction Gemini diffractometer was employed. Data were corrected for Lorentz polarization and absorption effects (empirical absorption correction SADABS).[28] Structures were solved by direct methods and refined by full-matrix least-squares based on all data using F^2.[29] H atoms were placed in calculated positions and refined isotropically using a riding model, except N-bonded hydrogens, which were located in the Fourier map and refined isotropically using the 1.2-fold U_{iso} value of the parent N atom; N−H distances were restrained to 0.89 Å (s.u. 0.02). All non-hydrogen atoms were refined with anisotropic displacement parameters. Similar U restraints were applied to the C, O, and N atoms of *fac*-[Re(phen)(CO)$_3$TbdzH][CF$_3$SO$_3$], *fac*-[Re(bpy)(CO)$_3$TcyaH][CF$_3$SO$_3$], and *fac*-[Re(bpy)(CO)$_3$TbdzH][CF$_3$SO$_3$] (s.u. 0.01). The O and F atoms of the $CF_3SO_3^-$ anion *fac*-[Re(phen)(CO)$_3$TphH][CF$_3$SO$_3$], *fac*-[Re(phen)(CO)$_3$TphH][CF$_3$SO$_3$]·0.25Et$_2$O, *fac*-[Re(phen)(CO)$_3$TcyaH][CF$_3$SO$_3$], *fac*-[Re(phen)(CO)$_3$TbdzH][CF$_3$SO$_3$], and *fac*-[Re(bpy)(CO)$_3$TbdzH][CF$_3$SO$_3$] were restrained to an isotropic-like behavior (ISOR line in SHELXL; s.u. 0.01). The Et$_2$O molecule in *fac*-[Re(phen)(CO)$_3$TphH][CF$_3$SO$_3$]·0.25Et$_2$O is disordered over four symmetry-related positions, and the independent image has been refined isotropically with a 0.25 occupancy factor.

CCDC-943783 (for *fac*-[Re(bpy)(CO)$_3$Tcya]), -943784 (for *fac*-[Re(phen)(CO)$_3$TphH][CF$_3$SO$_3$]), -943785 (for *fac*-[Re(phen)(CO)$_3$TphH][CF$_3$SO$_3$]·0.25Et$_2$O), -943786 (for −[Re(phen)(CO)$_3$TcyaH][CF$_3$SO$_3$]), -943787 (for *fac*-[Re(phen)(CO)$_3$TbdzH][CF$_3$SO$_3$]), -943788 (for *fac*-[Re(bpy)(CO)$_3$TcyaH][CF$_3$SO$_3$]), and -943789 (for −[Re(bpy)(CO)$_3$TbdzH][CF$_3$SO$_3$]) contain the supplementary crystallographic data for this paper. These data can be obtained free of charge from the Cambridge Crystallographic Data Centre via www.ccdc.cam.ac.uk/data_request/cif.

■ ASSOCIATED CONTENT

Ⓢ Supporting Information

X-ray crystallographic data for the complexes *fac*-[Re(bpy)(CO)$_3$Tcya], *fac*-[Re(phen)(CO)$_3$TphH][CF$_3$SO$_3$], *fac*-[Re(phen)(CO)$_3$TphH][CF$_3$SO$_3$]·0.25Et2O, *fac*-[Re(phen)(CO)$_3$TcyaH][CF$_3$SO$_3$], *fac*-[Re(phen)(CO)$_3$TbdzH][CF$_3$SO$_3$], *fac*-[Re(bpy)(CO)$_3$TcyaH][CF$_3$SO$_3$], and *fac*-[Re(bpy)(CO)$_3$TbdzH][CF$_3$SO$_3$] in CIF format. Table of bonding and angle parameters for *fac*-[Re(bpy)(CO)$_3$Tcya], crystal data and collection details for all the X-ray crystal structures described herein, ^{1}H NMR spectra of all the Re(I)-based species, emission spectra recorded at rt and at 77 K, and computational calculations. This material is available free of charge via the Internet at http://pubs.acs.org.

■ AUTHOR INFORMATION

Corresponding Authors

*E-mail: stefano.stagni@unibo.it.

*E-mail: m.massi@curtin.edu.au.

Notes

The authors declare no competing financial interest.

■ ACKNOWLEDGMENTS

M.V.W. and P.J.W. thank Curtin University and the Australian Government for funding through an APA. M.V.W. also thanks Boehringer Ingelheim Fonds for the Travel Grant and the Graduate Women (WA) for the Mary and Elsie Stevens Scholarship. P.R. thanks the Australian Research Council for funding his fellowship under the Discovery Program (DP0986999). P.R. and P.J.W. thank the National Computational Infrastructure for the provision of computer time. S.M. thanks the Italian Ministero dell'Istruzione, Università e Ricerca (M.I.U.R.)(PRIN 2009) for a Post-Doc grant. The Toso Montanari Foundation and the Australian Research Council are gratefully acknowledged for the financial support.

■ REFERENCES

(1) Campagna, S.; Puntoriero, F.; Nastasi, F.; Bergamini, G.; Balzani, V. *Top. Curr. Chem.* **2007**, *280*, 117−214.

(2) Kirgan, R. A.; Sullivan, B. P.; Rillema, D. P. *Top. Curr. Chem.* **2007**, *281*, 45−100.

(3) Flamigni, L.; Barbieri, A.; Sabatini, C.; Ventura, B.; Barigelletti, F. *Top. Curr. Chem.* **2007**, *281*, 143−203.

(4) (a) Grätzel, M. *Inorg. Chem.* **2005**, *44*, 6841−6851. (b) Hagfeldt, A.; Boschloo, G.; Sun, L.; Kloo, L.; Pettersson, H. *Chem. Rev.* **2010**, *110*, 6595−6663. (c) Yin, J.-F.; Velayudham, M.; Bhattacharya, D.; Lin, H.-C.; Lu, K.-L. *Coord. Chem. Rev.* **2012**, *256*, 3008−3035. (d) Bignozzi, C. A.; Argazzi, R.; Boaretto, R.; Busatto, E.; Carli, S.; Ronconi, F.; Caramori, S. *Coord. Chem. Rev.* **2013**, *257*, 1472−1492.

(5) (a) Holder, E.; Langeveld, B. M. W.; Schubert, U. S. *Adv. Mater.* **2005**, *17*, 1109−1121. (b) Yersin, H. *Highly Efficient OLEDs with Phosphorescent Materials*; Wiley-VCH: Weinheim, Germany, 2008. (c) Xiao, L.; Chen, Z.; Qu, B.; Luo, J.; Kong, S.; Gong, Q.; Kido, J.

Adv. Mater. **2011**, *23*, 926−952. (d) Fantacci, S.; De Angelis, F. *Coord. Chem. Rev.* **2011**, *255*, 2704−2726. (e) Costa, R. D.; Ortì, E.; Bolink, H. J.; Monti, F.; Accorsi, G.; Armaroli, N. *Angew. Chem., Int. Ed.* **2012**, *51*, 8178−8211.

(6) (a) Fernandez-Moreira, V.; Thorp-Greenwood, F.; Coogan, M. P. *Chem. Commun.* **2010**, *46*, 186−202. (b) Gill, M. R.; Thomas, J. A. *Chem. Soc. Rev.* **2012**, *41*, 3179−3192. (c) Salassa, L. *Eur. J. Inorg. Chem.* **2011**, 4931−4947. (d) Thorp-Greenwood, F.; Balasingham, R. G.; Coogan, M. P. *J. Organomet. Chem.* **2012**, *714*, 12−21.

(7) (a) Kumar, A.; Sun, S.-S.; Lees, A. J. *Coord. Chem. Rev.* **2008**, *252*, 922−939. (b) Otsuki, J.; Akasaka, T.; Araki, K. *Coord. Chem. Rev.* **2008**, *252*, 32−56. (c) Ma, D.-L.; Ma, V. P.-Y.; Chan, D. S.-H.; Leung, K.-H.; He, H.-Z.; Leung, C.-H. *Coord. Chem. Rev.* **2012**, *256*, 3087−3113.

(8) Wenger, O. S. *Chem.—Eur. J.* **2011**, *17*, 11692−11702 and references therein. See also: Kuss-Petermann, M.; Wolf, H.; Stalke, D.; Wenger, O. S. *J. Am. Chem. Soc.* **2012**, *134*, 12844−12854.

(9) Ruggi, A.; van Leeuwen, F. W. B.; Velders, A. H. *Coord. Chem. Rev.* **2011**, *255*, 2542−2554.

(10) (a) Mullice, L. A.; Pope, S. J. A. *Dalton Trans.* **2010**, *39*, 5908−5917. (b) Guerchais, V.; Fillaut, J.-L. *Coord. Chem. Rev.* **2011**, 2448−2457 and references therein. See also: (c) Ho, M.-L.; Cheng, Y.-M.; Wu, L.-C.; Chou, P.-T.; Lee, G.-H.; Hsu, F.-C.; Chi, Y. *Polyhedron* **2007**, *26*, 4886−4892. (d) Chang, S.-Y.; Chen, J.-L.; Chi, Y.; Cheng, Y.-M.; Lee, G.-H.; Jiang, C.-M.; Chou, P.-T. *Inorg. Chem.* **2007**, *46*, 11202−11212.

(11) (a) Massi, M.; Cavallini, M.; Stagni, S.; Palazzi, A.; Biscarini, F. *Mater. Sci. Eng., C* **2003**, *23*, 923−925. (b) Duati, M.; Tasca, S.; Lynch, F. C.; Bohlen, H.; Vos, J. G.; Stagni, S.; Ward, M. D. *Inorg. Chem.* **2003**, *42*, 8377−8384. (c) Zanarini, S.; Bard, A. J.; Marcaccio, M.; Palazzi, A.; Paolucci, F.; Stagni, S. *J. Phys. Chem. B* **2006**, *110*, 22551−22556. (d) Stagni, S.; Palazzi, A.; Zacchini, S.; Ballarin, B.; Bruno, C.; Marcaccio, M.; Paolucci, F.; Monari, M.; Carano, M.; Bard, A. J. *Inorg. Chem.* **2006**, *45*, 695−709. (e) Stagni, S.; Orselli, E.; Palazzi, A.; De Cola, L.; Zacchini, S.; Femoni, C.; Marcaccio, M.; Paolucci, F.; Zanarini, S. *Inorg. Chem.* **2007**, *46*, 9126−9138. (f) Stagni, S.; Palazzi, A.; Brulatti, P.; Salmi, M.; Muzzioli, S.; Zacchini, S.; Marcaccio, M.; Paolucci, F. *Eur. J. Inorg. Chem.* **2010**, 4643−4657. (g) Femoni, C.; Iapalucci, M. C.; Longoni, G.; Lovato, T.; Stagni, S.; Zacchini, S. *Inorg. Chem.* **2010**, *49*, 5992−6004.

(12) (a) Stagni, S.; Colella, S.; Palazzi, A.; Valenti, G.; Zacchini, S.; Paolucci, F.; Marcaccio, M.; Albuquerque, R. Q.; De Cola, L. *Inorg. Chem.* **2008**, *47*, 10509−10521. (b) Cocchi, M.; Kalinowski, J.; Muzzioli, S.; Stagni, S. *Appl. Phys. Lett.* **2009**, *94*, 083306−9.

(13) (a) Werrett, M. V.; Chartrand, D.; Gale, G. D.; Hanan, G. S.; MacLellan, J. G.; Massi, M.; Muzzioli, S.; Raiteri, P.; Skelton, B. W.; Silberstein, M.; Stagni, S. *Inorg. Chem.* **2011**, *50*, 1229−1241. (b) Silvester, D. S.; Uprety, S.; Wright, P. J.; Massi, M.; Stagni, S.; Muzzioli, S. *J. Phys. Chem. C* **2012**, *116*, 7327−7333. (c) Wright, P. J.; Muzzioli, S.; Werrett, M. V.; Raiteri, P.; Skelton, B. W.; Silvester, D. S.; Stagni, S.; Massi, M. *Organometallics* **2012**, *31*, 7566−7578. (d) Wright, P. J.; Muzzioli, S.; Skelton, B. W.; Raiteri, P.; Lee, J.; Koutsantonis, G.; Silvester, D. S.; Stagni, S.; Massi, M. *Dalton Trans.* **2013**, *42*, 8188−8191. (e) Wright, P. J.; Affleck, M. G.; Muzzioli, S.; Skelton, B. V.; Raiteri, P.; Silvester, D. S.; Stagni, S.; Massi, M. *Organometallics* **2013**, *32*, 3728−3737.

(14) MaGee, K. D. M.; Wright, P. J.; Muzzioli, S.; Siedlovskas, C. M.; Raiteri, P.; Baker, M. V.; Brown, D. H.; Stagni, S.; Massi, M. *Dalton Trans.* **2013**, *42*, 4233−4236.

(15) Durham, J. L.; Tirado, J. N.; Knott, S. A.; Oh, M. K.; McDonald, R.; Szczepura, L. F. *Inorg. Chem.* **2012**, *51*, 7825−7836.

(16) Butler, R. N. Tetrazoles. In *Comprehensive Heterocyclic Chemistry II*; Storr, R. C., Ed.; Pergamon Press: Oxford, U.K., 1996; Vol. *4*, pp 621−678, and references therein.

(17) Caspar, J. V.; Meyer, T. J. *J. Phys. Chem.* **1983**, *87*, 952−957.

(18) Yeh, S.-J.; Wu, M.-F.; Chen, C.-T.; Song, Y.-H.; Chi, Y.; Ho, M.-H.; Hsu, S.-F.; Chen, C. H. *Adv. Mater.* **2005**, *17*, 285−289.

(19) Frisch, M. J.; Trucks, G. W.; Schlegel, H. B.; Scuseria, G. E.; Robb, M. A.; Cheeseman, J. R.; Scalmani, G.; Barone, V.; Mennucci, B.; Petersson, G. A.; Nakatsuji, H.; Caricato, M.; Li, X.; Hratchian, H. P.; Izmaylov, A. F.; Bloino, J.; Zheng, G.; Sonnenberg, J. L.; Hada, M.; Ehara, M.; Toyota, K.; Fukuda, R.; Hasegawa, J.; Ishida, M.; Nakajima, T.; Honda, Y.; Kitao, O.; Nakai, H.; Vreven, T.; Montgomery, J. A., Jr.; Peralta, J. E.; Ogliaro, F.; Bearpark, M.; Heyd, J. J.; Brothers, E.; Kudin, K. N.; Staroverov, V. N.; Kobayashi, R.; Normand, J.; Raghavachari, K.; Rendell, A.; Burant, J. C.; Iyengar, S. S.; Tomasi, J.; Cossi, M.; Rega, N.; Millam, N. J.; Klene, M.; Knox, J. E.; Cross, J. B.; Bakken, V.; Adamo, C.; Jaramillo, J.; Gomperts, R.; Stratmann, R. E.; Yazyev, O.; Austin, A. J.; Cammi, R.; Pomelli, C.; Ochterski, J. W.; Martin, R. L.; Morokuma, K.; Zakrzewski, V. G.; Voth, G. A.; Salvador, P.; Dannenberg, J. J.; Dapprich, S.; Daniels, A. D.; Farkas, Ö.; Foresman, J. B.; Ortiz, J. V.; Cioslowski, J.; Fox, D. J. *GAUSSIAN 09* (Revision C.01); Gaussian, Inc.: Wallingford, CT, 2009.

(20) Crosby, G. A.; Demas, J. N. *J. Phys. Chem.* **1971**, *75*, 991−1024.

(21) Eaton, D. F. *Pure Appl. Chem.* **1988**, *60*, 1107−1114.

(22) Karstens, T.; Kobs, K. *J. Phys. Chem.* **1980**, *84*, 1871−1872.

(23) Miller, J. N. In *Standard in Fluorescence Spectrometry*; Chapman & Hall: London, 1981.

(24) (a) Becke, A. D. *Phys. Rev.* **1988**, *A38*, 3098−3100. (b) Becke, A. D. *J. Chem. Phys.* **1993**, *98*, 5648−5652. (c) Lee, C.; Yang, W.; Parr, R. G. *Phys. Rev.* **1988**, *B37*, 785−789.

(25) Andrae, D.; Haubermann, U.; Dolg, M.; Stoll, H.; Preub, H. *Theor. Chim. Acta* **1990**, *77*, 123−141.

(26) Tomasi, J.; Mennucci, B.; Cammi, R. *Chem. Rev.* **2005**, *105*, 2999−3093.

(27) (a) Palazzi, A.; Stagni, S.; Bordoni, S.; Monari, M.; Selva, S. *Organometallics* **2002**, *21*, 3774−3781. (b) Palazzi, A.; Stagni, S.; Selva, S.; Monari, M. *J. Organomet. Chem.* **2003**, *669*, 135−140.

(28) Sheldrick, G. M. *SADABS, Program for Empirical Absorption Correction*; University of Göttingen: Germany, 1996.

(29) Sheldrick, G. M. *SHELX97-Program for the Refinement of Crystal Structure*; University of Göttingen: Germany, 1997.